2

Steady One-Dimensional Detonations

Andrew Higgins

2.1 Introduction

While treatments of detonation wave propagation using control volume analysis, such as the Chapman–Jouguet (CJ) detonation solution presented in the prior chapter, are very successful in predicting the steady-state, equilibrium properties of detonations, they provide no information about the limits of detonation propagation or the dynamics of detonation waves. Addressing these issues necessitates investigating the structure of the detonation front. To illustrate this point, consider an extremely dilute concentration of fuel in air (e.g., 0.1% of methane in air by volume). If this mixture is entered into a thermochemical equilibrium code, a unique equilibrium CJ detonation solution will be generated. In practice, however, such a dilute mixture is highly unlikely to be able to support detonation wave propagation, since the low post-shock temperatures from the weak leading shock front would result in very slow reaction rates or no perceptible reaction at all. Even if exothermic reaction occurred, the long reaction zone would make the detonation susceptible to momentum and heat transfer losses at the boundaries of the wave (e.g., friction and cooling between the flow within the detonation front and the tube walls in the case of a confined detonation), which would ultimately quench the detonation. Thus, the issue of defining detonability limits naturally leads to an investigation of the reaction zone length.

To clarify the relation between the equilibrium solutions from the previous chapter and the detailed structure of the wave investigated in this chapter: The equilibrium solutions using the CJ criterion will accurately predict the detonation velocity and downstream thermodynamic state *if* a detonation occurs well inside its detonability limits and without losses. Such a control-volume analysis, however, cannot predict whether or not detonation will occur in a particular scenario. In other words, equilibrium calculations cannot be used to define detonability limits. Nor can equilibrium solutions be used to examine the initiation, transient dynamics, or stability of a detonation wave.

F. Zhang (ed.), *Shock Wave Science and Technology Reference Library, Vol. 6*: Detonation Dynamics, DOI 10.1007/978-3-642-22967-1_2,

A one-dimensional model for the structure of a steady detonation wave was developed independently by Zeldovich [106], von Neumann [58,59], and Döring [23] in the 1940s, although the concept of a detonation wave as an initial shock wave that initiates a combustion reaction was suggested as early as the end of the nineteenth century by Mikhel'son [57] and Vieille [98]. For the complete history of the development of detonation wave physics, see [5, 40, 48, 55]. The key assumption of the Zeldovich–von Neumann–Döring (ZND) model is that the leading shock front does not result in an immediate change in the chemical composition of the mixture; the chemistry is "frozen" across the leading shock front. The post-shock flow then reacts or "relaxes" to the final equilibrium solution determined by the CJ condition. The assumption that no reactions occur within the leading shock wave is well supported by the fact that shock waves are extremely thin, typically only a few mean free paths thick, while chemical reactions only occur occasionally upon molecular collisions. Thus, in gases, the chemical reactions occur on timescales many orders of magnitude greater than the shock, such that the chemistry across the shock is effectively frozen. For condensed-phase explosives, decomposition of the explosive molecule may begin on the scale of the shock front itself, but the energy release still occurs on a scale much longer than that of the shock, so the ZND representation remains applicable. The development and applications of the ZND framework are the subject of this chapter.

The ZND models of wave structure are represented schematically in Fig. 2.1. In a gaseous detonation, translational and rotational equilibrium is established extremely quickly following the arrival of the shock front. Vibrational excitation takes longer, but is still rapid compared to the overall reaction zone length and occurs with negligible chemical reaction. The majority of the reaction zone is dominated by a nearly thermally neutral process of chain initiating and chain branching chemical reactions, during which time a "soup" of radical species is built up. Significant exothermic reaction only occurs with recombination to product species (typically CO_2, H_2O, N_2, etc.), which happens relatively quickly in most reactive systems due to the feedback between heat evolution and the exponential dependence of reaction rates on temperature, finally leading to equilibrium at the sonic plane. The unsteady expansion of products beyond the sonic plane matches the product flow to the downstream boundary condition; this flow is treated in Appendix A.1.

For condensed phase (solid and liquid) explosives, the process is more complex and cannot as easily be classified into "nonreacting shock" and "reaction." Translational equilibrium is again established quickly on a length scale comparable to the explosive molecule itself, but vibrational excitation is a complex process owing to the polyatomic nature of most molecular explosives. The transfer of energy from low frequency to high frequency modes of molecular vibration is necessary to break molecular bonds (an endothermic process). The full details of this process are only now becoming accessible theoretically and experimentally. Recombination via chemical kinetics followed by vibrational de-excitation to stable, equilibrium products (again, CO_2, H_2O,

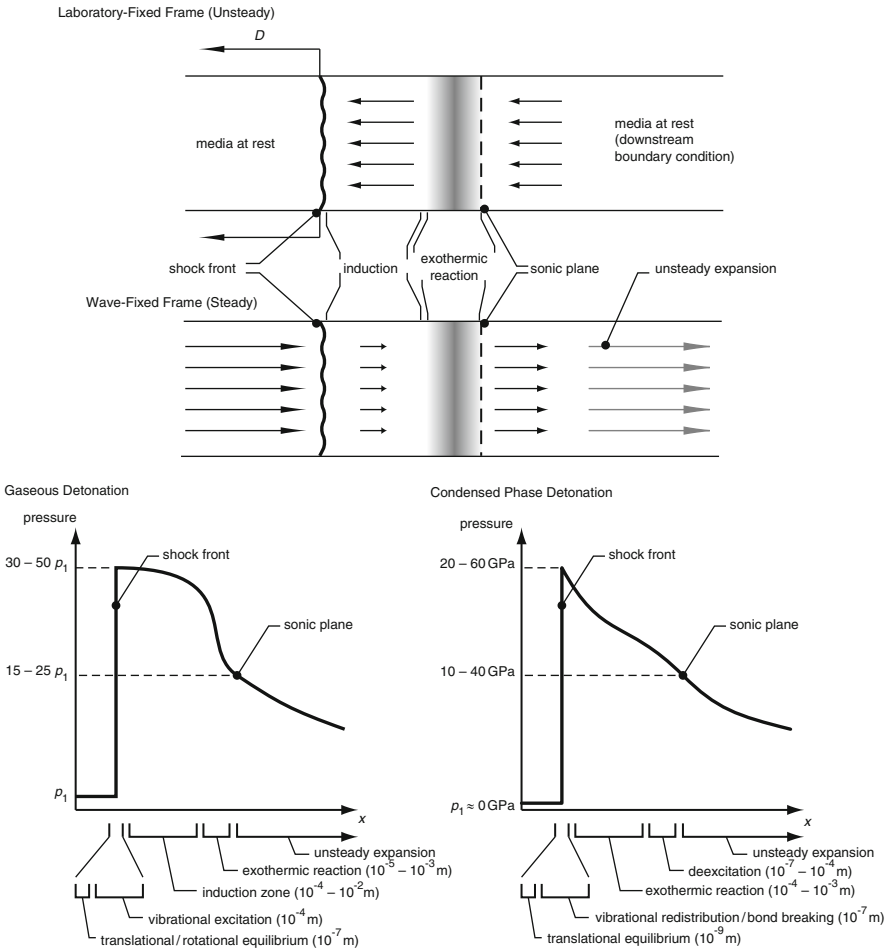

Fig. 2.1. Schematic of the ZND structure of a detonation wave, for both gaseous detonation at atmospheric conditions and condensed phase detonation

N_2, etc.) occurs as well as slower condensation and diffusion-controlled processes such as carbon particulate formation. A current picture of the Non-Equilibrium ZND (NEZND) structure of condensed phase detonation waves has been presented by Tarver [90, 92] and in Chap. 6 of this volume.

This picture is further complicated by the fact that all known gaseous detonations are hydrodynamically unstable (Chap. 3 of this volume) and this instability is manifested as a transient, three-dimensional cellular structure (see Chaps. 3–5 in this volume). Condensed-phase explosives are similarly complex. Most liquid explosives display a structure of transverse waves that are believed to be similar to those in gaseous detonation, only on a much finer scale. Solid explosives as used in most applications are polycrystalline,

resulting in the reaction zone structure being controlled by spatially localized reaction centers resulting from the heterogeneous nature of the media. All of these features mean that the steady, one-dimensional model considered in this chapter is highly idealized and typically cannot be used to make direct, quantitative predictions. Nevertheless, the general view of a prompt shock followed by a relatively long, thermally neutral induction process, and concluded with a rapid exothermic reaction, remains a valid picture for many detonation waves. Moreover, the steady, one-dimensional model of a detonation is of enormous value as an analytically tractable treatment of detonation waves, readily amenable to investigation and solution. More sophisticated models (i.e., transient and multidimensional) remain computationally challenging. Properly resolved one-dimensional numerical simulations of a gaseous detonation with realistic chemistry, for example, are at the boundary of what is feasible with state-of-the-art computers [67], and multidimensional simulations with fully resolved, detailed chemistry and molecular transport processes will likely remain beyond computational ability for some time.

2.2 ZND Model for Perfect Gas

For the ZND model of the reaction zone, it is necessary to integrate the differential form of the conservation laws coupled to a reaction rate equation, starting at the immediate post-shock or *von Neumann state*. The steady form of the conservation of mass, momentum, and energy written in conservative form

$$\mathrm{d}\left(\rho u A\right) = 0 \tag{2.1}$$

$$\mathrm{d}\left(p + \rho u^2\right) = -\rho u^2 \frac{\mathrm{d}A}{A} \tag{2.2}$$

$$\mathrm{d}\left(h + \frac{1}{2}u^2\right) = 0 \tag{2.3}$$

can be rewritten in differential form as

$$\frac{\mathrm{d}\rho}{\rho} + \frac{\mathrm{d}u}{u} + \frac{\mathrm{d}A}{A} = 0 \tag{2.4}$$

$$\mathrm{d}p + \rho u \mathrm{d}u = 0 \tag{2.5}$$

$$c_p \mathrm{d}T - \Delta q \mathrm{d}\lambda + u \mathrm{d}u = 0. \tag{2.6}$$

Here, λ is a *reaction progress variable*, where $\lambda = 0$ corresponds to unreacted mixture and $\lambda = 1$ is the fully reacted mixture. This system can be thought of as gas "A" that reacts exothermally to form "B" (i.e., global reaction A $\rightarrow$ B) with both gases being calorically perfect with the same heat capacity and molecular weight. The heat of reaction is $\Delta q = h^\circ_{f_\mathrm{A}} - h^\circ_{f_\mathrm{B}}$ and λ is the mass fraction of species "B." This simplified treatment of a reacting flow

is essentially Rayleigh flow or "Simple T_o-change flow" for a perfect gas, as developed in texts on compressible flow [74]. The enthalpy incorporates this heat release term similar to the enthalpy of formation in a real reacting system:

$$h = c_p T - \lambda \Delta q. \tag{2.7}$$

Finally, a differential form of ideal gas law ($p = \rho RT$) is also required

$$\frac{\mathrm{d}p}{p} = \frac{\mathrm{d}\rho}{\rho} + \frac{\mathrm{d}T}{T}. \tag{2.8}$$

By eliminating variables and introducing the sound speed $c^2 = \left(\frac{\partial p}{\partial \rho}\right)_s = \gamma RT$, the differential change in velocity is related to differential changes in the reaction progress variable and area

$$\frac{\mathrm{d}u}{u} = \frac{\frac{\Delta q}{c_p T}\mathrm{d}\lambda - \frac{\mathrm{d}A}{A}}{1 - \frac{u^2}{c^2}}. \tag{2.9}$$

Introducing the flow Mach number ($M = \frac{u}{c}$), this result can be written as

$$\frac{\mathrm{d}u}{u} = \frac{\frac{\Delta q}{c_p T}\mathrm{d}\lambda - \frac{\mathrm{d}A}{A}}{1 - M^2}. \tag{2.10}$$

If the flow is adiabatic or nonreacting ($\Delta q = 0$ or $\mathrm{d}\lambda = 0$), then a familiar result for isentropic compressible flow that relates the change in flow velocity to a differential change in area is obtained.

$$\frac{\mathrm{d}u}{u} = -\frac{\frac{\mathrm{d}A}{A}}{1 - M^2}. \tag{2.11}$$

For the remainder of this section, only constant area flow ($\mathrm{d}A = 0$) with exothermic heat release ($\Delta q > 0$) will be considered

$$\frac{\mathrm{d}u}{u} = \frac{\frac{\Delta q}{c_p T}\mathrm{d}\lambda}{1 - M^2}. \tag{2.12}$$

Comparing (2.11) and (2.12), it can be seen that heat addition, much like converging area in steady isentropic flow, drives the flow toward sonic by accelerating a subsonic flow or decelerating a supersonic flow. The presence of the $1 - M^2$ term in the denominator raises the question as to what happens when the flow reaches Mach 1. In order to prevent a singularity in (2.12), the differential change in the reaction progress variable $\mathrm{d}\lambda$ must also be zero as the flow becomes sonic. Usually, this condition corresponds to equilibrium when the flow composition has finished evolving. Again, there is an analogy to isentropic compressible flow, where sonic flow ($M = 1$) can only occur at a locally constant cross-sectional area ($\mathrm{d}A = 0$).

The rate at which chemical reactions release heat into the flow can be modeled by an Arrhenius expression

$$\dot{\lambda} = k(1-\lambda)\exp\left(-\frac{E_a}{RT}\right), \tag{2.13}$$

where the $1-\lambda$ term ensures that the reaction rate decreases to zero as the initial reactant is entirely consumed. The activation energy E_a in the Arrhenius expression will be seen to have a determining role in the structure of the reaction zone.

This rate equation refers to the reaction of a fluid element or particle in the flow. It can be related to the spatial derivative of λ using the particle derivative:

$$\dot{\lambda} = \frac{D\lambda}{Dt} = \frac{\partial\lambda}{\partial t} + u\frac{\partial\lambda}{\partial x}. \tag{2.14}$$

Since the wave-fixed frame is assumed to be steady state in the ZND model, $\frac{\partial\lambda}{\partial t} = 0$, so

$$\frac{\mathrm{d}\lambda}{\mathrm{d}x} = \frac{1}{u}\dot{\lambda}. \tag{2.15}$$

The governing differential equation for the flow velocity through the reaction zone becomes

$$\frac{\mathrm{d}u}{\mathrm{d}x} = \frac{\frac{\Delta q}{c_p T}\dot{\lambda}}{1-M^2}. \tag{2.16}$$

Equations (2.13), (2.15), and (2.16) form a coupled set of ordinary differential equations. In addition, the temperature must be computed at any point in the flow given a value of $u(x)$ and $\lambda(x)$. This can be done via the energy equation

$$T(x) = \frac{1}{c_p}\left(c_p T_1 + \lambda(x)\Delta q + \frac{1}{2}\left(u_1^2 - u(x)^2\right)\right), \tag{2.17}$$

where T_1 and u_1 are the initial temperature and velocity of the flow approaching the detonation before encountering the shock wave ($u_1 = D$). The sound speed (as required to compute Mach number) is given by $\sqrt{\gamma RT}$. This set of (2.13), (2.15)–(2.17) can be numerically integrated, starting from the post-shock von Neumann state ($x = 0$), which is determined by the normal shock relations. The Mach number of the leading shock front can be computed using the relations for a CJ detonation, as given by

$$M_{\mathrm{CJ}} = \sqrt{(\gamma+1)\frac{\Delta q}{c_p T_1} + 1 + \sqrt{\left[(\gamma+1)\frac{\Delta q}{c_p T_1} + 1\right]^2 - 1}}. \tag{2.18}$$

Alternatively, the value of the initial shock Mach number can be guessed and iterated upon until a numerical solution for the reaction zone is found that satisfies the requirement that the reaction reaches equilibrium ($\lambda = 1$) as

the flow becomes sonic. Either of these approaches will yield the same solution, unless a "pathological" case is encountered, as discussed in the following sections.

Numerical integration of the reaction zone structure was carried out for three cases, $\frac{E_a}{RT_1} = 10$, 25, and 50, and the results plotted in Fig. 2.2. For these calculations, $Q = \frac{\Delta q}{c_p T_1} = 10$ and $\gamma = 1.2$. The value of k in the rate equation (2.13) was set to unity (alternatively, since k has units of 1/s, it is possible to define a nondimensional time $\hat{t} = kt$). Note that, given the form of the rate equation (2.13), the equilibrium state of $\lambda = 1$ will, in principle, never be reached and can only be approached asymptotically. Thus, it is difficult to define a reaction zone length where the heat release is complete. Rather, some other definition of reaction zone length must be used. Common choices are the half-reaction zone length (variously defined as where $\lambda = 0.5$, where half of the heat addition occurs, or where temperature reaches the midpoint

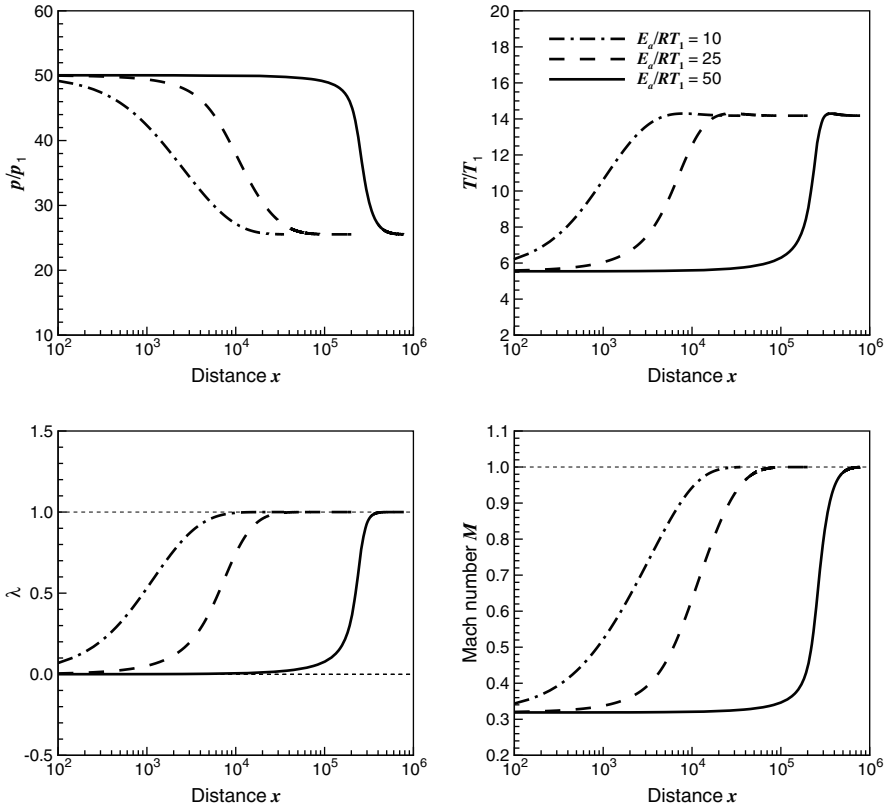

Fig. 2.2. Structure of ZND detonation, showing pressure, temperature, reaction progress variable, and flow Mach number for various values of activation energy $\frac{E_a}{RT_1}$, $Q = 10$, $\gamma = 1.2$. Note the use of log scale for x-axis

between T_{vN} and T_{CJ}), the location of the maximum reaction rate, or the inflection point of the temperature profile.

As activation energy is increased from $\frac{E_a}{RT_1} = 10$ to $\frac{E_a}{RT_1} = 25$, the reaction zone increases by an order of magnitude in length. Increasing from $\frac{E_a}{RT_1} = 25$ to $\frac{E_a}{RT_1} = 50$ results in an additional two orders of magnitude increase in reaction zone length. The length scale of these reaction zones is somewhat arbitrary, due to taking the value of k as unity. What is more significant is the increasing *sharpness* of the reaction profile as activation energy is increased. A lower activation energy results in a relatively gradual increase in temperature beginning immediately after the shock, while the high activation energy results in a long plateau of nearly constant conditions followed by a comparatively rapid energy release. This feature of high activation energy reflects the underlying temperature sensitivity of chemical reactions that must be activated and is one of the most significant and reoccurring themes in the development of detonation theory.

The temperature profiles in Fig. 2.2 feature maxima that occur before the end of the reaction zone; this is most clearly visible in the temperature profile for the $\frac{E_a}{RT_1} = 50$ case due to the steepness of the profile but it is present in all cases plotted. Beyond this maximum, exothermic heat release in the flow has the effect of lowering the temperature. This counterintuitive result is a consequence of the heat release resulting in greater flow acceleration and pressure/density reduction than its contribution to raising the static temperature of the flow. This temperature decrease with heat addition occurs when the Mach number is in the range $\frac{1}{\sqrt{\gamma}} < M < 1$; this result is well established in compressible one-dimensional flow with heat addition (Rayleigh flow).

It is interesting to explore what happens if a calculation of the reaction zone structure is initialized with a non-CJ detonation velocity. This is done in Fig. 2.3 for $\frac{E_a}{RT_1} = 25$, where the solution was initialized with the post-shock state for shock Mach numbers 20% greater and 20% less than the CJ Mach number. For the stronger shock case, the reaction zone structure can be solved for, and as the reaction progress variable reaches $\lambda = 1$, the flow is seen to remain subsonic. This solution corresponds to a strong detonation, i.e., the branch of the product Hugoniot curve above the CJ detonation point on the (p, v) plane. This case is also referred to as an overdriven detonation, since the detonation is being forced to propagate at a speed greater than the CJ speed, and the heat release is insufficient to choke the flow. If the solution is initialized with a sub-CJ detonation velocity, the numerical integration encounters a singularity as the flow becomes sonic while the reaction rate is still finite ($\lambda < 1$) in (2.16). In this case, the heat release is sufficient to choke the flow before adding the full heat release, and further heat addition to a sonic flow is not permitted in a steady solution. This singularity will appear for any initial condition that is even infinitesimally less than the CJ speed. A similar result is obtained if the wave speed is fixed and the heat release Q increased incrementally. The appearance of a mathematical singularity may

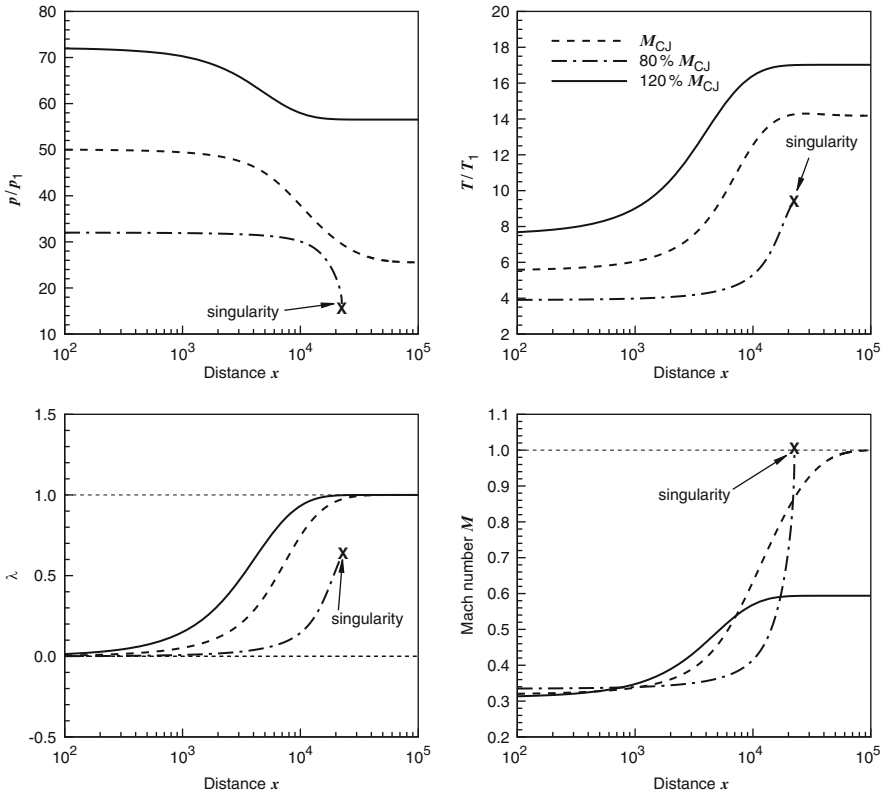

Fig. 2.3. Structure of ZND detonation for reaction zone structure initialized with a CJ detonation, a detonation overdriven at 120% M_{CJ}, and a shock at 80% M_{CJ} showing pressure, temperature, reaction progress variable, and flow Mach number for $\frac{E_a}{RT_1} = 25$, $Q = 10$, $\gamma = 1.2$. The sub-CJ shock does not correspond to a solution of conservation laws, resulting in a singularity appearing in the numerical integration

appear alarming, but recall that the CJ detonation is the minimum velocity wave consistent with the governing conservation laws. The fact that a singularity is encountered in numerically integrating through the reaction zone initialized with a speed less than the minimum speed simply reflects that an attempt is being made to solve a flow using initial conditions for which no steady solution exists.

2.3 Pathological Detonations

Instead of the one step reaction A → B, consider a two-step reaction with A reacting to form B, which in turn reacts to form C

$$\text{Reaction 1:} \quad \mathrm{A} \rightarrow \mathrm{B} \tag{2.19}$$

$$\text{Reaction 2:} \quad \mathrm{B} \rightarrow \mathrm{C} \tag{2.20}$$

with the first reaction being exothermic ($\Delta q_1 > 0$), the second reaction being endothermic ($\Delta q_2 < 0$), and the overall reaction exothermic ($|\Delta q_2| < \Delta q_1$). The solution of the reaction zone structure in this case becomes a more complicated problem. Specifically, initializing the differential equations for the reaction zone using the CJ detonation velocity based on the final, equilibrium heat release of the overall reaction ($\Delta q_{\text{tot}} = \Delta q_1 + \Delta q_2$) results in a singularity being encountered as the integration proceeds. In this case, it is necessary to guess and iterate on the value of detonation velocity in order to find a wave velocity that permits the governing differential equations to yield a well-behaved solution. This solution, called the *eigenvalue detonation solution*, may occur whenever there are competing effects influencing the flow in the detonation reaction zone. The particular scenario encountered here, in which a detonation velocity greater than the CJ velocity based on the total heat release is obtained due to an endothermic reaction, is called *pathological detonation*.

To explore the structure of a detonation with competing exothermic and endothermic reactions, the system A $\rightarrow$ B $\rightarrow$ C will be considered with the two reaction steps governed by Arrhenius rate laws

$$\dot{\lambda_1} = k(1-\lambda_1)\exp\left(-\frac{E_{a1}}{RT}\right) \qquad \dot{\lambda_2} = k(\lambda_1-\lambda_2)\exp\left(-\frac{E_{a2}}{RT}\right), \tag{2.21}$$

where λ_1 and λ_2 are the reaction progress variables for the reaction A $\rightarrow$ B and B $\rightarrow$ C, respectively. The mass fractions of A, B, and C are given by

$$Y_{\text{A}} = 1-\lambda_1 \qquad Y_{\text{B}} = \lambda_1 - \lambda_2 \qquad Y_{\text{C}} = \lambda_2. \tag{2.22}$$

This set is a highly simplified analog to a real, multi-step chemical kinetic mechanism, where the reaction must pass through an intermediate species B in order to produce the final product C.

The differential equation governing the reaction zone is now

$$\frac{\mathrm{d}u}{\mathrm{d}x} = \frac{\frac{1}{c_pT}(\Delta q_1\dot{\lambda_1} + \Delta q_2\dot{\lambda_2})}{1-M^2}, \tag{2.23}$$

which is the two-step analog to (2.16). Equation (2.17) must be similarly modified to account for the two-step reaction.

This system was proposed by Fickett and Davis [19] and its dynamics further explored by Sharpe and Falle [75, 77]. For this system, the activation energy and heats of reaction are assigned as follows:

$$\frac{E_{a1}}{RT_1} = 25 \qquad \frac{E_{a2}}{RT_1} = 25 \tag{2.24}$$

$$Q_1 = \frac{\Delta q_1}{c_pT_1} = 20 \qquad Q_2 = \frac{\Delta q_2}{c_pT_1} = -10. \tag{2.25}$$

Note that the overall reaction has a net heat release of $Q_{\text{tot}} = Q_1 + Q_2 = 10$, the same as the system considered previously. Thus, the CJ detonation Mach

number based on the equilibrium heat release is $M_{\mathrm{CJ}_{\mathrm{equil}}} = 6.781$. Initializing the integration of (2.23) with the von Neumann state based on this shock Mach number results in a singularity being encountered, as shown in Fig. 2.4. It is necessary to increase the shock Mach number to $M_{\mathrm{CJ}_{\mathrm{eigen}}} = 7.207$ (or approximately 6% greater than the CJ speed based on equilibrium) in order to find a solution that does not encounter a singularity within the reaction zone structure. This value can only be found by trial and error integration of the governing ordinary differential equations. The term Chapman–Jouguet is still used to refer to this solution, since it features a sonic surface consistent with Jouguet's original criterion. To differentiate these two cases, they will be referred to as the CJ equilibrium solution and the CJ eigenvalue solution. Finally, to eliminate any confusion as to why the presence of an *endothermic* reaction results in a *greater* than equilibrium detonation velocity, note that the detonation velocity associated with the first stage exothermic reaction alone would be $M_{\mathrm{CJ}}(Q_1) = 9.486$. The endothermic reaction reduces the effective heat release and detonation velocity in comparison to this value, but the pathological behavior results in a detonation velocity that is greater than the CJ equilibrium solution based on the total heat release.

Numerical integration of ordinary differential equations with a potential singularity embedded within the solution is a notoriously difficult problem. It may be necessary to intervene in the numerical algorithm used in order to select a solution, since upon encountering the sonic point, the differential equations become indeterminate. Alternatively, it is possible to start at the sonic point and integrate forward, toward the shock. Even in this case, iteration is still required to find a solution consistent with the initial conditions upstream of the wave, since the thermodynamic state of the sonic point is not known a priori.

For the solution of the governing ordinary differential equations initialized with $M_{\mathrm{CJ}_{\mathrm{eigen}}} = 7.207$, the solution for the reaction zone structure is shown in Fig. 2.4. Coincident with the sonic point, the local heat release rate is seen to go to zero due to an exact balance between the rate of exothermic heat addition and endothermic heat removal. This condition is referred to as the *generalized Chapman–Jouguet condition*, a term first used by Eyring et al. [27]. The condition of the local heat release rate being zero behaves like a quasi-equilibrium condition in (2.23), enabling the solution to pass smoothly through the sonic point and proceed downstream as a supersonic flow (recall that heat removal accelerates a supersonic flow away from sonic). This case is shown as the heavy, solid line in Fig. 2.4.

The sonic point of the generalized CJ condition is a *saddle point*, so in principle it is also possible for the solution at the sonic point to return to the subsonic branch under the influence of subsequent endothermic reaction, as shown by the thin, dashed lines in Fig. 2.4. This solution, however, features a nonphysical "kink" in the flow properties. Thus, it could be suggested that the solution that passes smoothly from the subsonic to the supersonic branch is the correct one, but this cannot be proven rigorously. As mentioned previously,

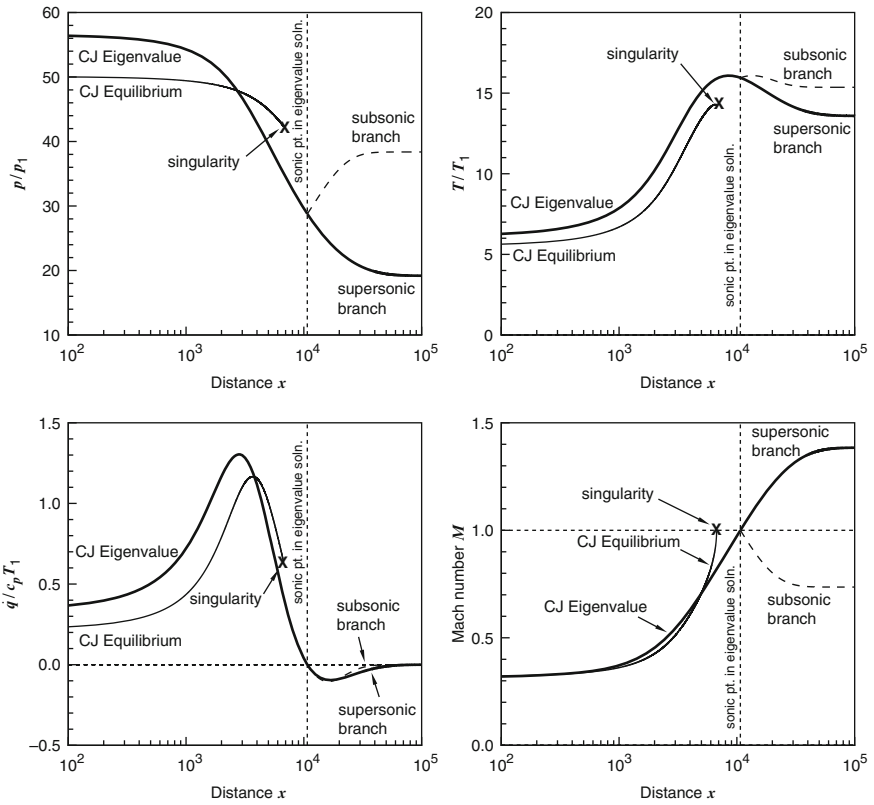

Fig. 2.4. Reaction zone structure of ZND detonation with a two-step, exothermic/endothermic system, showing pressure, temperature, heat release rate, and flow Mach number for $\frac{E_{a1}}{RT_1} = \frac{E_{a2}}{RT_1} = 25$, $Q_1 = 20$, $Q_2 = -10$, $\gamma = 1.2$. The reaction zone initialized with a shock based on the CJ equilibrium solution encounters a singularity in the numerical integration. The eigenvalue solution can pass smoothly through the sonic point, resulting in supersonic flow at the end of the reaction zone (weak detonation)

similar indeterminacy occurs in compressible isentropic flow when an initially subsonic flow becomes sonic at an area minimum (i.e., at a throat). If the requirement that the flow properties at the throat vary smoothly is imposed, the flow should transition to a supersonic solution locally at the throat, and from there, the flow can either continue supersonically or return to the subsonic branch via a shock wave, depending on the downstream boundary condition (e.g., back pressure).

For both the detonation with competing reactions and isentropic flow with area change, the issue of resolving which branch of the solution following the sonic point is the correct solution is ultimately determined by considering the downstream boundary condition. Establishing how the flow exiting the sonic

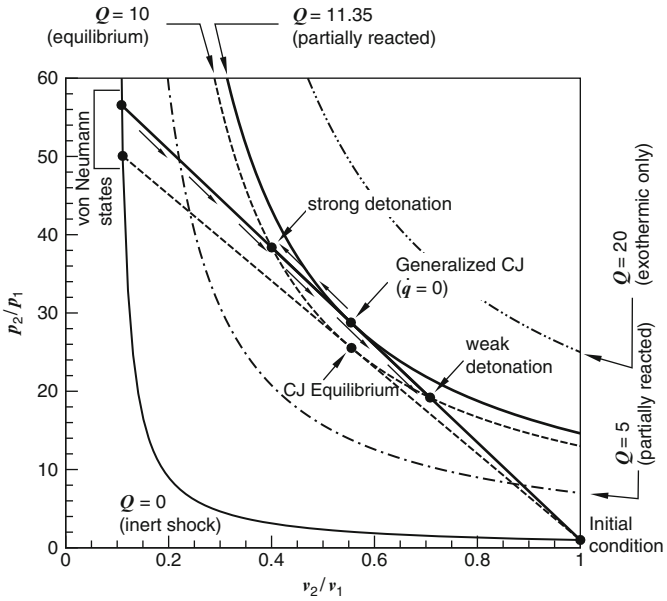

Fig. 2.5. Equilibrium and eigenvalue solutions for a two-step, exothermic/endothermic system visualized in the (p, v) plane ($\frac{E_{a1}}{RT_1} = \frac{E_{a2}}{RT_1} = 25$, $Q_1 = 20$, $Q_2 = -10$, $\gamma = 1.2$)

surface of such a detonation matches with a downstream condition imposed by a piston becomes quite involved as a number of possible scenarios need to be considered. The reader is referred to the book by Fickett and Davis [19] for a complete exposition on this problem. Fickett and Davis also consider the case of two exothermic reactions, which turns out to be qualitatively similar to a single exothermic reaction and does not exhibit pathological behavior. For the most frequently encountered case of a downstream piston at rest (corresponding to a detonation in a close-ended tube, for example), the flow passes smoothly to the supersonic solution beyond the sonic point. In this case, the leading edge of the rarefaction wave lags behind the sonic surface and the end of the reaction zone, resulting in a region of uniform supersonic flow between the end of the reaction zone and the leading rarefaction that will increase in size as the detonation propagates. These scenarios are discussed further in Appendix A.1.

The eigenvalue solution can also be interpreted in the (p, v) plane with the use of partially reacted Hugoniots, as first proposed by von Neumann [58].[1] In Fig. 2.5, the Hugoniot and Rayleigh line for the equilibrium solution are shown as dashed lines. The Hugoniots for the value of heat release at an intermediate

[1] Formally, a Hugoniot is a locus of possible equilibrium end states for a steady wave, so a "partially reacted Hugoniot" is a misnomer.

value ($Q = 5$) and at the sonic point of the eigenvalue solution ($Q = 11.35$) are plotted as dashed-dotted and solid lines, respectively. The Rayleigh line for the eigenvalue solution is seen to be tangent to the solid Hugoniot curve at the point where the net rate of heat release is zero (the generalized CJ condition). In actuality, there is a continuous series of partially reacted Hugoniots, and the correct one to use for the detonation solution cannot be determined until the kinetic rate equation has been integrated, as was done above. Starting from the von Neumann point, as the reaction progresses, the solution proceeds down the Rayleigh line as indicated by the directional arrows. At the sonic point of the eigenvalue solution, the solution is indeterminate. As endothermic reactions dominate over the exothermic beyond the sonic point, the solution may continue down the Rayleigh line (supersonic branch), or may proceed back up the Rayleigh line (subsonic branch). Either branch of the solution eventually reaches the equilibrium Hugoniot. The upper intersection point can be recognized as a *strong detonation* and the lower intersection as a *weak detonation*. As discussed above, the weak solution is more likely to be realized, and thus pathological detonations are an example of a weak detonation solution. If the reaction zone calculation is initialized with the post-shock state corresponding to the CJ equilibrium solution (dashed straight line), then as the tangency condition (sonic flow) is encountered for the first time, the net heat release rate is still positive. As net exothermic reaction continues, there is no longer an intersection between the Rayleigh line and the partially reacted Hugoniot, resulting in the singularity encountered in Fig. 2.4. Thus, it is not possible to construct a trajectory of partially reacted states to reach the CJ equilibrium solution. Detonations for which the equilibrium CJ detonation solution may not be the correct solution (or permissible solution) due to competing effects in the reaction zone may occur in systems with real chemistry as well (Sect. 2.5).

2.4 Detonations with Source Terms

In order to discuss limits to detonation propagation, losses must be introduced into the governing conservation equations. In a system without losses and governed by an Arrhenius-type reaction rate, detonation propagation is always possible due to the following mechanism. An Arrhenius-governed system will inevitably react to equilibrium, and the temperature increase from even a weak shock wave will accelerate the reaction, resulting in a wave of exothermic energy release traveling with the shock some distance behind it. In the case of a very slow reaction, this front of exothermicity may be spatially separated from the shock by vast distances, but in the absence of losses such as heat transfer or friction, the energy released will eventually feed into supporting the shock, ultimately resulting in a detonation. (Recall that a CJ detonation is the minimum velocity allowed for a steady, compressive combustion wave;

lower velocity combustion waves are not permitted by the conservation laws.) This concept is sometimes referred to in the Russian detonation literature as *Khariton's principle*, namely that any media capable of exothermic reaction is capable of supporting detonation wave propagation in the absence of losses [72]. Thus, any discussion of the limits to detonation propagation must include the effects of losses.

The steady, one-dimensional mass, momentum, and energy equations including friction and heat transfer source terms in the wave-fixed reference frame are

$$\mathrm{d}\left(\rho u\right) = 0 \tag{2.26}$$

$$\mathrm{d}\left(p + \rho u^2\right) = f\mathrm{d}x \tag{2.27}$$

$$\mathrm{d}\left[\rho u\left(h + \frac{1}{2}u^2\right)\right] = q\mathrm{d}x + fu_1\mathrm{d}x, \tag{2.28}$$

where f is a source term of momentum and q is a source term of energy. The velocity u_1 is the velocity of the wall in the wave-fixed frame, which is equal in magnitude to the velocity of the wave in the laboratory-fixed frame, D. As written here, f and q are the volumetric source terms, with units of $[\mathrm{N\,m^{-3}}]$ and $[\mathrm{W\,m^{-3}}]$, respectively. A mass source term could also be included to account for, for example, mass loss into a porous wall; however, this effect is usually treated by introducing area divergence into the governing equations, as discussed in Sect. 2.6. These momentum and energy sources will be related to wall friction and heat transfer coefficients below. Note the appearance of the friction term f in the energy equation, representing the work done by friction. The significance of this term will be elaborated upon in Sect. 2.4.2 below. Following the development of Sect. 2.2, a differential equation for the flow velocity in the reaction zone can be found

$$\frac{\mathrm{d}u}{\mathrm{d}x} = \frac{\frac{\Delta q\dot{\lambda}}{c_pT} + \frac{q}{\rho c_pT} + \frac{f(u_1(\gamma-1)-\gamma u)}{\rho c^2}}{1-M^2}. \tag{2.29}$$

Note that if $f = 0$ and $q = 0$, (2.29) reverts back to (2.16). Heat transfer to the wall is a heat loss ($q < 0$), so inspecting (2.29) reveals that the effect of heat loss is similar to that of endothermic reactions studied in the previous section. Heat losses will result in the detonation propagating at speeds less than the ideal CJ detonation velocity (i.e., a detonation without losses), and determining the solution will necessitate iterating on the propagation velocity until a regular solution of the reaction zone structure can be found. The effect of friction is not as intuitive, due to the terms of mixed sign involving f in (2.29); however, it will be shown that friction also results in a velocity deficit in comparison to the ideal CJ velocity.

2.4.1 Source Terms

For a detonation in a tube with wall friction, the source term f represents the frictional force at the wall spread over the entire cross-sectional area of the tube. Thus, f is given by

$$f = \frac{\tau_w P}{A}, \tag{2.30}$$

where τ_w is the shear stress at the wall and P the wetted perimeter of the tube. Introducing the hydraulic radius $r_h = \frac{2A}{P}$ and the skin friction coefficient

$$c_f = \frac{\tau_w}{\frac{1}{2}\rho u_{\text{rel}}^2}, \tag{2.31}$$

where u_{rel} is the velocity relative to the wall, and this term becomes

$$f = \rho(u - u_1)|u - u_1|\frac{c_f}{r_h}. \tag{2.32}$$

The absolute value operator ensures that friction always opposes the motion of the flow relative to the wall. Of course, there exists an enormous literature on correlations for the friction coefficient c_f, relating it to Reynolds number, surface roughness, etc. For highly turbulent flows ($Re > 10^6$) typically encountered in detonation waves, the friction coefficient is usually in the range of 0.01–0.001.

The heat source term is given by

$$q = -h_c(T - T_w)\frac{P}{A}, \tag{2.33}$$

where h_c is the heat transfer coefficient and T_w is the wall temperature. The minus sign reflects that heat transfer out of the system is a loss. The heat transfer coefficient may be related to the friction coefficient c_f via the Reynolds analogy, which states that for a turbulent flow the transport of heat and momentum are via the same underlying mechanism, as follows:

$$h_c = c_p \rho |u_1 - u| \frac{c_f}{2}. \tag{2.34}$$

The relative velocity between the flow and the wall is used since the main mechanism of heat transfer is forced convection. The Reynolds analogy is expected to be valid in the case of a media with a ratio of viscous to thermal transport, as expressed by the Prandtl number $\text{Pr} = \frac{\mu c_p}{k}$ (μ is viscosity, k thermal conductivity), that is of order unity. For most gases ($\text{Pr} \approx 0.8$), thus, this analogy is expected to hold. This assumption allows the heat transfer and friction source terms to be expressed in terms of a single nondimensional parameter, c_f. Using these expressions in (2.29), the differential equation for velocity becomes

$$\frac{\mathrm{d}u}{\mathrm{d}x} = \frac{\frac{\Delta q}{c_p T}\dot{\lambda} - \frac{c_f}{r_h}|u_1 - u|\left(\frac{T - T_w}{T}\right) - \frac{c_f}{r_h}\frac{(u_1 - u)|u_1 - u|(\gamma u - (\gamma - 1)u_1)}{c^2}}{1 - M^2}. \tag{2.35}$$

This equation can now be integrated to obtain the structure of the reaction zone with friction and heat losses. Note that the friction coefficient c_f always appears in combination with the hydraulic radius r_h. Also note that (2.17), which relates temperature to the flow velocity, can no longer be used due to the source term in the energy equation. A separate differential equation for temperature must be coupled to the solution of (2.35); such an equation can be found by using the differential equation of state (2.8).

2.4.2 Work Done by Friction

The presence of a work term due to friction in the energy equation and the fact that this term makes a positive contribution to energy (similar in sign to exothermic heat release) may appear counterintuitive and has been the source of some apprehension in implementing the ZND model for detonations with friction. This confusion is compounded by the fact that in one-dimensional compressible adiabatic flow with friction (i.e., Fanno flow), this term is absent [74]. This matter was explored at some length by Tanguay and Higgins [88] and is briefly recounted here in hopes of clarifying this issue.

Traditional Fanno flow in a tube is formulated in the laboratory-fixed reference frame, where the tube walls are stationary. Within the one-dimensional framework, the fluid in the tube moves at a single velocity at a given cross-sectional area along the tube, and thus the shear force τ_w at the wall would do work on the fluid (just as friction acting on a block sliding across a stationary table top does work on the block). However, this work term is excluded from the energy equation in Fanno flow in recognition of the no-slip boundary condition known to apply in viscous fluids. Thus, excluding the work term in the Fanno relations is a means to incorporate the multidimensional no-slip condition into a one-dimensional model.

In the ZND model of a detonation, the model is formulated in the wave-fixed reference frame, where the walls will be moving at speed D (the same speed at which the wave propagates into quiescent gas in the laboratory-fixed reference frame). In this case, the shear force τ_w acting on the fluid at the wall is undergoing a displacement at a rate D in the same direction as the shear force acts, so positive work is being done. As a result of this energy input by friction, the velocity deficits observed in detonation wave propagation with friction are not as great as would be computed by just including friction losses in the momentum equation alone (although a velocity deficit compared to a detonation with no friction still exists).

The question naturally arises, where does this energy come from? This question is addressed via a simple thought experiment proposed by Tanguay and Higgins and illustrated schematically in Fig. 2.6. Beginning with the propagating detonation wave in the laboratory-fixed reference frame (Fig. 2.6a), the wave can be rendered steady by transforming into a coordinate system attached to the wave (Fig. 2.6b). Now, suppose that it is desired wish to study

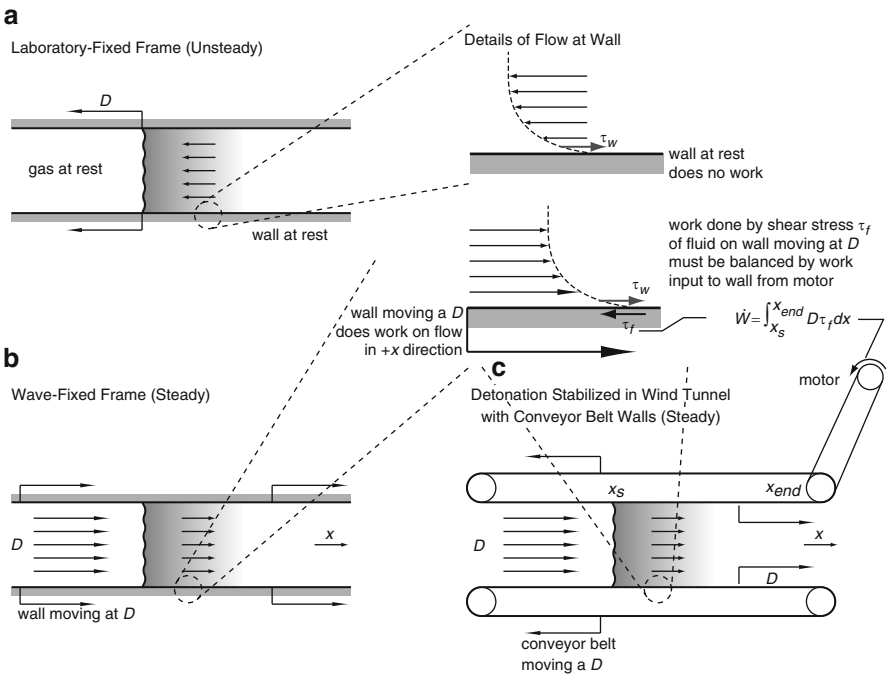

Fig. 2.6. A schematic illustrating the origin of the work term in the energy equation for detonations with friction. (**a**) Laboratory-fixed (unsteady) reference frame, in which no work is done by friction. (**b**) In the wave-fixed (steady) reference frame, in which the wall shear stress does work on the fluid due to displacement of the force. (**c**) Detonation stabilized in a wind tunnel with moving, conveyor-belt walls that equal the speed of the upstream flow. Work must be input to the conveyor belt via a motor to offset the drag due to friction acting on the conveyor belt

a detonation wave propagating in a tube under steady conditions in the laboratory. This could be done by stabilizing the detonation in a wind tunnel, where a flow of explosive gas is fed into the test section at a velocity equal to the detonation velocity, stabilizing the wave in the test section. In order to perfectly simulate a detonation propagating in a stationary tube, it would be necessary to make the walls of the wind tunnel move at the detonation velocity as well; this could be done by making the walls out of a conveyor belt, as shown in Fig. 2.6c. From the perspective of the detonation wave, the three arrangements in Fig. 2.6 are identical. For the detonation stabilized in the wind tunnel, in the region of the detonation reaction zone, the fluid will act via shear stress to slow down the conveyor belt, and thus to maintain a steady picture, a source of work must be put into the conveyor belt (e.g., by using an electric motor) which is then transferred to the fluid. Thus, while there is no work input from friction to the unsteady detonation wave in Fig. 2.6a, there *is* a work input from friction to the steady detonation wave in Fig. 2.6c,

and therefore in Fig. 2.6b as well. This situation, where work is present in one reference frame and not in another, is commonly encountered in mechanics.

As a final proof, it is possible to start from a laboratory-fixed reference frame and, using the full unsteady Euler equations with friction, simulate a propagating detonation wave that moves through the computational domain. In this reference frame, no work is done since the no-slip boundary condition is assumed to apply and the walls are at rest, although there is a loss term in the momentum equation due to friction. Such a calculation was done by Dionne et al. [22], and the resulting wave propagation was shown by Tanguay and Higgins [88] to agree with the steady-state analysis where the work term was included in the energy equation and to significantly disagree with the steady-state analysis where the work term was excluded. Thus, in order to properly model a steady detonation in the one-dimensional ZND framework, the work input term due to friction must be included in (2.28).

2.4.3 Effect of Friction

While the Reynolds analogy, as discussed in the previous section, suggests that heat transfer will always be accompanied by friction, and vice versa, it is advantageous to examine each of these effects individually. Examining friction by itself is an approximation to a detonation occurring in an obstacle-laden channel or in an explosive gas mixture filling the interstitial spaces of a solid porous media, where momentum losses may dominate over heat transfer losses.

The effect of friction alone was studied by guessing the detonation wave velocity and then iterating on the governing ODE (2.35) with the heat transfer term removed until an eigenvalue solution could be obtained. The wave velocity found by this method is plotted in Fig. 2.7 as a function of the friction coefficient to hydraulic radius ratio $\frac{c_f}{r_h}$, along with profiles of the reaction wave structure for a few select cases. An activation energy of $E_a = 32$ was used for this figure, and the half reaction zone length of a detonation without losses, denoted $L_{1/2}$, was used to nondimensionalize the hydraulic radius and the distance from the shock front. For the case of no friction ($c_f = 0$), the same solution as studied in Sect. 2.2 is obtained, which propagates at a Mach number of 6.781. The addition of a momentum loss due to friction results in a wave velocity that is less than the CJ velocity without losses. As the value of the friction coefficient is increased (or the tube radius decreased), a lower post-shock temperature results in the reaction zone length becoming longer, making the wave even more susceptible to momentum losses. The fact that the sonic point is encountered before the complete energy is released also contributes to the increasing velocity deficit; however, this effect can be shown to be negligible in comparison to the influence of the momentum losses on the detonation velocity. As the value of $\frac{c_f L_{1/2}}{r_h}$ approaches $\approx$0.01, the decrease in wave velocity becomes increasingly steep until a *turning point* is encountered,

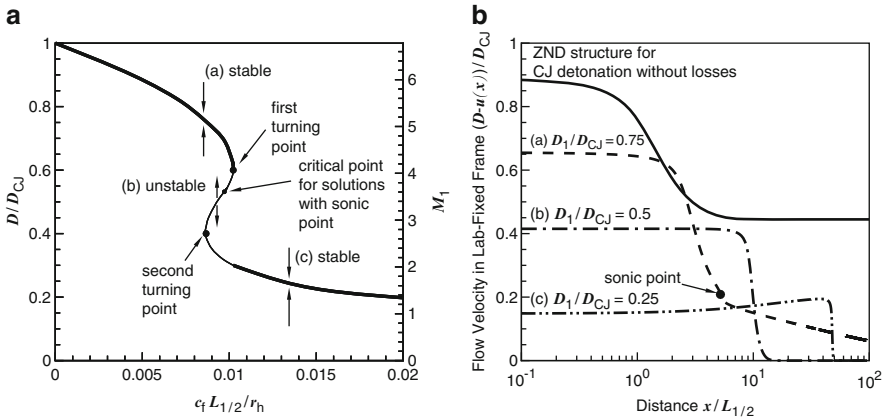

Fig. 2.7. ZND detonation with friction (no heat loss) for $\frac{E_a}{RT_1} = 32$, $Q = 10$, and $\gamma = 1.2$. (**a**) Wave velocity and Mach number as a function of the friction coefficient c_f. (**b**) Structure of the wave, showing as the flow velocity relative to the fixed wall. Hydraulic radius r_h and distance x are nondimensionalized by the half reaction zone length of detonation without losses $L_{1/2}$

at which point the wave is propagating at about 60% of the CJ velocity without losses for the particular activation energy studied here. Further decreasing the wave velocity below the turning point gives rise to the second branch of the solution curve in Fig. 2.7 that is denoted with a thin line, and for a given value of $\frac{c_f L_{1/2}}{r_h}$, the solution curve becomes multivalued in this region. As discussed below, the branch of the solution with a positive slope (i.e., increasing wave velocity with increasing friction) is believed to be unstable and cannot be physically realized.

As the detonation wave velocity is decreased further, at a certain point the flow velocity exiting the wave equals the velocity of flow approaching the wave. At velocities below this critical condition, a sonic point can no longer be located. The detonation wave velocity at this critical point can be solved analytically (see Appendix A.2) as

$$M_{\mathrm{crs}} = \frac{D_{\mathrm{crs}}}{c_1} = \sqrt{\gamma Q + 1}, \tag{2.36}$$

where "crs" denotes the critical sonic point. As viewed from the laboratory-fixed frame, this solution corresponds to a front of constant volume explosion conditions moving into unreacted mixtures at the sound speed of the combustion products. This result is independent of the details of the reaction zone structure such as the reaction rate.

To continue the solution curve below the critical sonic point, a new criterion is adopted, namely that the flow exiting the wave must be at rest in the laboratory-fixed reference frame. This corresponds to the condition of a

detonation propagating in a close-ended tube that imposes zero flow velocity at the end of the reaction zone ($D - u = 0$), as shown in cases (b) and (c) in Fig. 2.7b. That the downstream boundary condition now influences the wave propagation reflects the fact that the flow exiting the wave is entirely subsonic with respect to the wave. As the wave velocity decreases further, a second turning point is encountered. Further increasing the friction coefficient $\frac{c_f}{r_h}$ results in a decreasing detonation wave velocity. The length of detonation wave reaction zone in this regime becomes very long, about two orders of magnitude longer than the ideal detonation wave without losses, for the case shown in Fig. 2.7c owing to the low post-shock temperatures ($M_1 = 1.5$ for case (c)). A wave with such a long reaction zone length is unlikely to be observed experimentally; however, it may qualitatively correspond to the low velocity "choking regime" as discussed in Sect. 2.4.5 below.

The stability of the various branches can now be considered. Since discussion of the stability of a detonation wave implies its transient response to a perturbation, it is outside the scope of the steady analysis presented in this chapter. However, following Zeldovich and Kompaneets [107], it is possible to present a heuristic argument for why the region of the solution curve with a positive slope (i.e., increasing velocity with increasing friction coefficient) should not be physically realizable, as follows. It can be shown that steady reaction zone structures initialized with conditions to the left of the solution curve correspond to a situation where the effect of heat release is greater than the effect of friction in comparison to the solution on the curve. In regions to the right of the curve, friction dominates over heat release, resulting in the flow remaining subsonic through the reaction zone. Thus, if a wave starting on the solution curve at point (a) in Fig. 2.7 was artificially perturbed downward to a lower velocity, attempts to solve for the reaction zone structure would result in a singularity as the heat release prematurely brings the flow to sonic. It can be conjectured that in a transient simulation, this perturbation that increases the influence of heat release in comparison to friction would have the effect of accelerating the wave, returning it to the solution curve. Likewise, artificially increasing the wave velocity at point (a) would result in friction having an increased influence, such that the flow velocity remains subsonic through the entire reaction zone (no sonic point), making the wave susceptible to rarefactions from behind that would decelerate the wave back to the solution curve. Thus, the upper branch of the solution curve in Fig. 2.7 can be hypothesized as a stable attractor.

Once past the turning point, where the slope of the detonation velocity with respect to friction becomes positive, the scenario is reversed, and a perturbation in wave velocity downward brings the wave into a region where the influence of heat release is diminished as compared to friction, reducing the wave speed further. A perturbative increase in wave speed would increase the influence of heat release over friction, resulting in the wave accelerating away from this branch of the solution curve. Thus, it is concluded that this branch of the solution is unstable. Once below the critical sonic point, a sonic

condition can no longer be found, but similar considerations apply. To the left of the solution curve below the critical sonic point, the flow velocity leaving the wave is negative (meaning, into the end wall), which would have the effect of accelerating the wave due to the reflected compression generated. To the right of the solution curve, the flow velocity is away from the end wall, and the resulting rarefaction generated would decelerate the wave. Thus, the region of the curve with positive slope is also unstable below the critical point as well.

The behavior conjectured here was verified by numerical simulations of the transient problem performed by Dionne et al. [20,22]. Numerical solutions of the unsteady one-dimensional Euler equations with momentum and energy source terms initialized with the steady, ZND structures found here in the region of positive slope (i.e., between the two turning points) quickly developed an instability after propagating only a few half reaction zone lengths and promptly jumped to the upper branch of the solution and then propagated indefinitely. Thus, the upper branch of the solution appears to be stable, although for sufficiently high activation energy, the numerical simulations of Dionne et al. exhibited pulsations such that the wave speed oscillated around the steady-state value found here. The simulations of Dionne et al. also found that solutions initialized with the steady ZND structure for the multivalued region of the solution curve below the second turning point were also unstable and promptly jumped to the upper branch of the solution (while our ad hoc analysis above would suggest that waves in this region could be stable). Only for values of the friction coefficient large enough to bring the solution curve into a region where it is again single valued did Dionne et al. find stable solutions in their transient simulations. Thus, only the sections of the solution curve shown with a thick line in Fig. 2.7a are believed to correspond to steady (or quasi-steady), realizable waves.

The backward "S" shape of the wave velocity as a function of the friction coefficient will be seen to be characteristic of all detonations with losses and, in a larger picture, flame models incorporating losses as well [85], provided the energy release rate has the strong temperature dependence of activated reactions (i.e., Arrhenius kinetics). The upper turning point is usually identified as the point of wave failure or abrupt transition to a regime of lower propagation velocity, with the other branches of the solution in the multivalued region being unstable. This behavior reflects the observed failure of detonation waves due to losses, wherein a deficit in velocity grows with increasing losses until an abrupt drop to a low velocity detonation (LVD) is observed, corresponding to encountering the first turning point and dropping onto the lowest branch of the solution. For lower values of activation energy E_a, it is theoretically possible for the wave velocity to remain a single valued function of friction and to decrease smoothly and monotonically; however, these values of E_a are not representative of real detonable gases. Reaction rate models with low thermodynamic state sensitivity appear in the modeling of condensed-phase explosives, and in these cases the detonation velocity can decrease monotonically without a critical point as well.

2.4.4 Effect of Heat Loss

The effect of heat transfer alone is examined in Fig. 2.8a, where the eigenvalue velocity of detonation is shown for different values of activation energy. The detonation velocity is plotted as a function of the heat transfer parameter, which is represented by the product of the friction coefficient c_f (which determines the heat transfer coefficient via the Reynolds analogy, even though friction has been switched off for these particular calculations) and the ratio of half reaction zone length (for a CJ detonation) to the tube hydraulic radius. Qualitatively, the results are very similar to those in which friction is examined in isolation (i.e., without heat transfer) as was shown in Fig. 2.7. Specifically, in the region to the left of the solution curve, heat generation is greater than heat loss, such that a singularity is encountered, and the region to the right of the solution curve is where heat loss dominates, such that the flow remains subsonic. Again, this feature of the solution can be used to suggest that only the upper branch of the solution is realizable. Thus, the turning point (denoted as a dot in Fig. 2.8a) is the critical value of heat transfer and detonation velocity at which detonation failure occurs. The different solution curves for different values of activation energy show that greater values of E_a, indicating a greater temperature sensitivity of the reaction zone, cannot tolerate large velocity deficits from the CJ velocity before they fail, while lesser

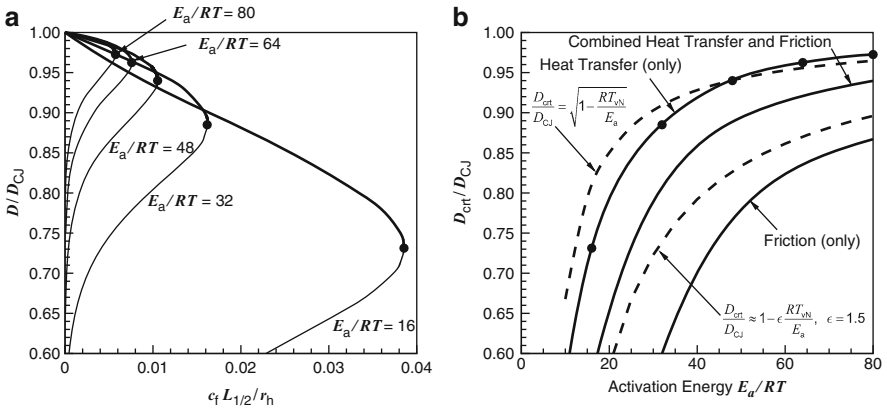

Fig. 2.8. (**a**) Detonation velocity as a function of the heat transfer parameter, with the stable branch shown as a *heavy line*, the nonphysical branch as a *thin line*, and the critical turning points denoted as *dots*, for different values of activation energy. (**b**) Detonation velocity at the critical turning point as a function of activation energy for detonations with different loss mechanisms. *Solid curves* are derived from iteration of numerical integrations of the reaction zone structure to find the eigenvalue detonation solution at the critical turning point, with the *dots* denoting critical points found in (**a**). *Dashed curves* derive from an activation energy asymptotic analysis [107, 109, 110]

values of E_a can exhibit larger velocity deficits. The dependence of the critical detonation velocity upon activation energy is shown in Fig. 2.8b.

For the case of heat transfer without friction losses, Zeldovich and Kompaneets [107] were able to solve analytically for the dependence of the velocity deficit from the CJ value by exploiting the fact that flow properties initially vary slowly behind the shock wave and can be taken as constant until the temperature becomes close to the value at the end of the reaction zone and the heat release occurs extremely rapidly. This approach has since been formalized into a methodology known as *activation energy asymptotics*. Zeldovich and Kompaneets found the following relation for the velocity at the critical turning point conditions

$$\frac{D_{\mathrm{crt}}}{D_{\mathrm{CJ}}} = \sqrt{1 - \frac{1}{\left(\frac{E_a}{RT_{\mathrm{vN}}}\right)}}, \tag{2.37}$$

where "crt" denotes critical turning point. The post-shock temperature of the CJ detonation without losses can be used for the von Neumann temperature T_{vN}. This relation can be approximated as

$$\frac{D_{\mathrm{crt}}}{D_{\mathrm{CJ}}} \approx 1 - \frac{1}{2}\frac{1}{\left(\frac{E_a}{RT_{\mathrm{vN}}}\right)}. \tag{2.38}$$

This curve is shown in Fig. 2.8b as a dashed line and exhibits remarkably good agreement with the value of critical velocity obtained via iteration upon numerical integration of the reaction zone structure in order to find the critical conditions, particularly for larger values of activation energy E_a.

Also shown in Fig. 2.8b are the values of critical velocity at the turning point for the case with friction alone (as was considered in Sect. 2.4.4) and the combined effect of friction and heat transfer. Detonations with frictional losses alone are able to tolerate larger velocity deficits for the same activation energy; this feature is attributed to the work input to the energy equation from friction, as discussed in Sect. 2.4.2, which has the effect of assisting to sustain the reaction in comparison to heat transfer losses. Detonation models including both friction and heat transfer exhibit intermediate velocity deficits at critical conditions, between friction and heat transfer individually. Zeldovich et al. [109, 110] suggested a general form of the velocity deficit relation

$$\frac{D_{\mathrm{crt}}}{D_{\mathrm{CJ}}} \approx 1 - \epsilon\frac{1}{\left(\frac{E_a}{RT_{\mathrm{vN}}}\right)}, \tag{2.39}$$

where ϵ has suggested values in the range of 0.9–1.8 for detonations with combined heat transfer and friction for physically relevant values of E_a ($\epsilon = 1.5$ is shown in the figure), with $\epsilon \to 0.5$ as $E_a \to \infty$ and thus converging to (2.38). As seen from Fig. 2.8b, the values of activation energy must be made

very large (i.e., beyond values that correspond to real reactive systems) in order to see this convergence. In Sect. 2.6, the same relation relating velocity deficit to activation energy will be found to apply to detonations with front curvature due to lateral flow divergence from yielding confinement.

Detonations with large frictional and heat transfer losses, as would be encountered in porous media for example, have been extensively studied theoretically by Sivashinsky and colleagues in recent years [6–9, 11, 35, 43]. Their work has further elucidated the structure of the reaction front and classified the possible modes of propagation, particularly low velocity (including subsonic) regimes. Their modeling, similar to that presented here, used a single-step Arrhenius kinetics reaction mechanism. As discussed in the next subsection, this reaction model is likely not relevant to the actual mechanism of burning in reactive waves with large losses. Models that attempt to incorporate the contribution of turbulent combustion to the reaction mechanism by using greatly exaggerated values of transport properties (e.g., effective turbulent diffusivity, etc.) may provide a future direction to link these models with experimental results [11].

2.4.5 Experiments with Losses

Gaseous detonations in channels that exhibit large velocity deficits due to momentum and heat transfer losses to wall roughness or obstacles have been extensively studied and are referred to as *quasi-detonations*. Quasi-steady propagation at velocities as low as 50% of the ideal CJ velocity has been observed. Reviews of results of these studies can be found in [32] and Chap. 7 of [51]. It is unlikely that planar shock-initiated homogeneous reactions contribute significantly to the energy release in such detonations. Calculations performed with detailed chemistry show that the reaction rates for the low shock velocities involved are much too slow to result in exothermic reactions on the timescales of the observed quasi-detonations. A seminal study by Shchelkin [78] suggested that shock reflection off obstacles in the tube may generate local hot spots that initiate reaction and thus enable the detonation to continue propagating at speeds for which a planar shock would not be of sufficient strength to sustain propagation. Much of the framework for explaining detonation phenomena in gaseous and condensed phase explosives has since been built around this "hot spot" idea. In addition, it is likely that interactions of the post-shock flow with the obstacles, the boundary layer that forms on the tube wall, and the turbulent nature of the quasi-detonation front itself all contribute to burning the mixture and sustaining the front. The mechanism of propagation of very high speed ($>300\,\mathrm{m\,s^{-1}}$) turbulent flames has not been convincingly elucidated and currently comprises a "no man's land" between premixed turbulent combustion and detonation, which includes the transition between the two (deflagration to detonation transition) [14, 52]. As such, models to address the reaction mechanism are ad hoc and semi-empirical in nature

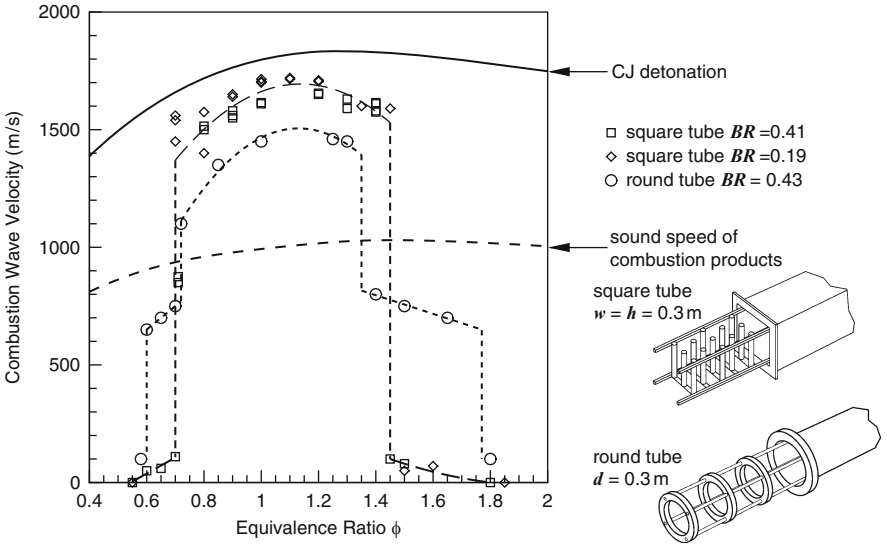

Fig. 2.9. Experiments examining detonations with propane/air mixtures in obstacle-laden channels (1 atm initial pressure). As the mixture equivalence ratio becomes sufficiently rich or lean, the longer reaction zone thickness increases momentum losses until detonation wave undergoes an abrupt transition to a lower velocity choking regime (*circular tube*) or low velocity flame (*square tube*) [12, 65]

and will not be discussed here; see [32, 109, 110] for a discussion of models that attempt to reproduce the reaction zone of detonations in rough tubes.

The main contribution to understanding quasi-detonation propagation by the type of model presented here is qualitative in nature, particularly the appearance of a critical velocity that can lead to the abrupt transition to a regime of lower propagating velocity. As an example, consider the experimental results of Peraldi et al. [65] and Chao and Lee [12] (see Fig. 2.9), which show the propagation velocity of detonation in propane/air mixtures in obstacle-laden channels . The specific geometry was either a square channel with staggered cylindrical pillars or a circular tube with annular rings, with the obstacle spacing approximately one channel height or tube diameter and with a blockage ratio denoted BR, defined as the cross-sectional area of the obstacle divided by the cross-sectional area of the channel or tube. As the mixture equivalence ratio ϕ was made rich or lean in comparison to stoichiometry, the reaction zone length increased, in turn increasing the relative momentum and heat transfer losses to the detonation wave. For the circular tube, as the equivalence ratio reached a value of $\phi \approx 0.8$ or $\phi \approx 1.4$, there was an abrupt transition to a lower velocity regime of propagation comparable to the sound speed in the combustion products (sometimes called the "choking regime"). This behavior is qualitatively similar to encountering the turning point of the "backwards S" curve in Fig. 2.7. These findings, however,

are geometry dependent, as seen in the results with the square tube with staggered pillars, which while exhibiting a critical velocity did not exhibit a transition to the low velocity choking regime. Similar studies of detonations in gaseous mixtures filling the interstitial spaces in packed beds of inert spherical beads by Makris et al. [53, 54] and Pinaev and Lyamin [66] failed to identify a critical velocity for a large number of different explosive mixtures, with a continuous spectrum of propagation velocity from the ideal CJ velocity down to 30% of the CJ velocity. It is likely that the role of turbulent mixing-driven combustion waves accounts for the geometry-depending velocity deficit and critical behavior that cannot be predicted by the simple homogeneous reaction mechanisms with exponential temperature dependence used in this chapter.

2.5 Systems with Real Chemistry

In order to have a more accurate model for real systems, it is necessary to take into account the details of the chemical reactions, rather than simply treating the energy release of reaction as external heat addition as was done in prior sections. In this section, a model of a steady, one-dimensional detonation in a reacting system of ideal gases will be developed, following the developments found in [67, 73]. This analysis begins with the same differential form of the conservation equations (2.1)–(2.3) and additional conservation equations for each individual chemical species

$$\mathrm{d}\left(\rho_i u A\right) = W_i \dot{\omega} A \mathrm{d}x \tag{2.40}$$

since species will be produced and consumed while chemical reactions proceed. The i subscript in (2.40) denotes a particular chemical element or compound. The $\dot{\omega}$ term is the rate of species production via chemical reaction (units: kmol/m^3-s), and W_i is the molecular weight of species i. It is convenient to introduce the mass fraction of a species $Y_i = \frac{\rho_i}{\rho}$, where ρ is the density of the mixture. Under the assumption of the Dalton model of partial pressure, the ideal gas law applies to each individual species $\left(p_i = \rho_i \frac{R_u}{W_i} T\right)$. The average molecular weight of the mixture (which will, in general, not remain constant as the mixture reacts) is given by

$$\frac{1}{W} \equiv \sum_i \frac{Y_i}{W_i}. \tag{2.41}$$

The enthalpy term h contains both the sensible enthalpy and the latent enthalpy of formation. Thus, it is not necessary to introduce a heat release term into the energy equation to account for exothermic chemical reaction. Specifically, h is given by

$$h = \sum_i \left(h_{f_i}^{\circ} + \int_{298.15}^{T} c_{p_i}(\theta) \mathrm{d}\theta \right) Y_i, \tag{2.42}$$

where $h^\circ_{f_i}$ is the enthalpy of formation of species i at the reference state (298.15 K and 1 atm). The enthalpy of formation is the energy absorbed (or released) when a given species is synthesized from the most stable form of its constituent elements. By definition, h°_f for the stable form of the elements at standard conditions ($T_{\text{ref}} = 298.15\,\text{K}, p_{\text{ref}} = 1\,\text{atm}$) is zero. A positive enthalpy of formation indicates that a species absorbs energy in its formation; a negative enthalpy of formation indicates that energy is released in the formation of the species. This assumption provides a consistent reference state that takes into account the energy absorbed (or liberated) as chemical bonds are broken (or formed) in a reacting system. The integral term in (2.42) gives the sensible enthalpy change relative to the reference state. Here, θ is introduced as a dummy variable of integration. The numerical values for enthalpy of formation and specific heat as a function of temperature may be obtained from the JANAF thermochemical tables [13], which have been conveniently curve fit with polynomials by [34, 56].

In order to formulate an ODE that can be integrated through the ZND reaction zone, the differential form of the governing conservation equations and the equation of state are used

$$\frac{\mathrm{d}\rho}{\rho} + \frac{\mathrm{d}u}{u} + \frac{\mathrm{d}A}{A} = 0 \tag{2.43}$$

$$\mathrm{d}p + \rho u \mathrm{d}u = 0 \tag{2.44}$$

$$\mathrm{d}h + u\mathrm{d}u = 0 \tag{2.45}$$

$$\frac{\mathrm{d}p}{p} = \frac{\mathrm{d}\rho}{\rho} - \frac{\mathrm{d}W}{W} + \frac{\mathrm{d}T}{T}. \tag{2.46}$$

The dh term can be expanded as follows:

$$\mathrm{d}h = \sum_i \left(h^\circ_{f_i} + \int_{298.15}^{T} c_{p_i}(\theta)\mathrm{d}\theta \right) \mathrm{d}Y_i + \sum_i Y_i \mathrm{d}\left(\int_{298.15}^{T} c_{p_i}(\theta)\mathrm{d}\theta \right). \tag{2.47}$$

The first term can be denoted $-\mathrm{d}q$

$$\mathrm{d}q \equiv -\sum_i \left(h^\circ_{f_i} + \int_{298.15}^{T} c_{p_i}(\theta)\mathrm{d}\theta \right) \mathrm{d}Y_i. \tag{2.48}$$

This is the usual definition of *enthalpy of combustion* (also called *heat of reaction*), which is the difference between the enthalpy of the products and the reactants at a fixed temperature and pressure.

The differential in the second term of (2.47) can be written as

$$\mathrm{d}\left(\int_{298.15}^{T} c_{p_i}(\theta)\mathrm{d}\theta \right) = c_{p_i}\mathrm{d}T. \tag{2.49}$$

Note that in bringing the differential under the integral, c_{p_i} is a monovariant function of temperature (i.e., Leibniz's Rule for differentiation under the integral sign is not required).

The mass-fraction weighted sum of these terms gives the mixture average heat capacity at constant pressure with frozen chemical composition c_{p_f}

$$c_{p_f} \equiv \left(\frac{\partial h}{\partial T}\right)_{p,Y_i} \equiv \sum_i Y_i c_{p_i}. \tag{2.50}$$

The subscript f is used for properties that derive from partial derivatives where the chemical composition is held fixed.

Thus, the differential from of the conservation of energy can be written very compactly as

$$c_{p_f} \mathrm{d}T - \mathrm{d}q + u\mathrm{d}u = 0. \tag{2.51}$$

Eliminating $\mathrm{d}\rho$, $\mathrm{d}P$, and $\mathrm{d}T$ from the differential form of the conservation relations and equation of state

$$\frac{\mathrm{d}u}{u} = \frac{\frac{\mathrm{d}q}{c_{p_f}T} - \frac{\mathrm{d}W}{W} - \frac{\mathrm{d}A}{A}}{1 - \left(\frac{1}{\frac{R_u}{W}} + \frac{1}{c_{p_f}}\right)\frac{u^2}{T}}. \tag{2.52}$$

Further introducing the frozen heat capacity at constant volume

$$c_{v_f} \equiv \left(\frac{\partial e}{\partial T}\right)_{v,Y_i} \equiv \sum_i Y_i c_{v_i} \tag{2.53}$$

and that the frozen heat capacities are related by

$$c_{p_f} - c_{v_f} = \frac{R_u}{W}. \tag{2.54}$$

Introducing a frozen composition isentropic exponent γ_f

$$\gamma_f = \frac{c_{p_f}}{c_{v_f}}. \tag{2.55}$$

Note that, in general, $c_p - c_v \neq R$ for a reacting gas [60]. The relations here (2.54) are only valid for the special case where the composition is assumed frozen. Introducing the frozen speed of sound (discussed in Sect. 2.5.4 below)

$$c_f = \sqrt{\gamma_f \frac{R_u}{W} T} \tag{2.56}$$

then the result found above (2.52) can be written as

$$\frac{\mathrm{d}u}{u} = \frac{\frac{\mathrm{d}q}{c_{p_f}T} - \frac{\mathrm{d}W}{W} - \frac{\mathrm{d}A}{A}}{1 - \left(\frac{u}{c_f}\right)^2}. \tag{2.57}$$

Introducing the frozen Mach number as the ratio of the flow velocity to the local frozen speed of sound ($M_f = \frac{u}{c_f}$)

$$\frac{\mathrm{d}u}{u} = \frac{\frac{\mathrm{d}q}{c_{p_f}T} - \frac{\mathrm{d}W}{W} - \frac{\mathrm{d}A}{A}}{1 - M_f^2}. \tag{2.58}$$

The similarity of this relation to (2.12) for the perfect gas model is clear, where the additional $\frac{\mathrm{d}W}{W}$ term reflects the changing chemical composition. In order for the solution to pass through a sonic point in the flow and avoid a singularity, the numerator must simultaneously go to zero, i.e., the following condition must be satisfied

$$\frac{\mathrm{d}q}{c_{p_f}T} - \frac{\mathrm{d}W}{W} - \frac{\mathrm{d}A}{A} = 0 \quad \text{when} \quad M_f = 1. \tag{2.59}$$

This condition is the *generalized CJ criterion* for a detonation with detailed chemical reactions. For a constant area flow, the numerator in (2.58) is sometimes referred to as the *thermicity* parameter, denoted σ [19].

$$\sigma = \frac{\mathrm{d}q}{c_{p_f}T} - \frac{\mathrm{d}W}{W}. \tag{2.60}$$

Thermicity can be defined as the influence of chemical reaction on flow velocity (or, via the momentum equation, pressure) due to both chemical energy release and an increase or decrease in the number of moles present. The appearance of the variable molecular weight term provides another possibility for a pathological (or eigenvalue) detonation: the exothermic heat release may exactly balance the decrease in the number of moles as the mixture reacts, resulting in the thermicity going to zero before equilibrium has been established.

The significance of the appearance of the frozen (as opposed to the) sound speed will be discussed in Sect. 2.5.4. It should be mentioned that, although it is the frozen sound speed that appears in the final equation (2.58), at no point was it assumed that the frozen sound speed is the "correct" sound speed to use. Rather, c_f appeared naturally in the governing equations, specifically in (2.52). It was not necessary to explicitly introduce c_f. In fact, the original ODE's (2.43)–(2.47) could be numerically integrated directly, without any manipulation to produce the form of (2.58). However, integration of this set of ODE's for an arbitrary initial von Neumann state would result in encountering a singularity in the solution in some cases. Further examination of the solution would reveal that this singularity occurs as the local flow velocity equals the frozen sound speed with finite thermicity. Only in the case where the flow velocity equals the frozen sound speed as the thermicity goes to zero (i.e., a saddle point) can the solution pass through the sonic point. The form of (2.58) makes this requirement clear.

2.5.1 Chemical Reaction Rates

In order to complete the model of a steady, one-dimensional detonation with real chemistry, the species source term $\dot{\omega}$ must be specified. For a generic

reaction A + B → C + D, the rate at which reactions occur in a unit volume is given by:

$$\dot{\omega} = C_{\mathrm{A}} C_{\mathrm{B}} k_{\mathrm{f}}, \tag{2.61}$$

where C_{A} and C_{B} are the molar concentrations of species A and B, respectively. Their product is proportional to the likelihood of collisions, which are a necessary prerequisite to reactions. The k_{f} term is the forward reaction rate constant given by the Arrhenius form

$$k_{\mathrm{f}} = AT^{n} \exp\left(\frac{E_a}{R_u T}\right). \tag{2.62}$$

Here A is a pre-exponential factor that includes the collision cross section of the atoms or molecules and a steric factor that takes the geometry of the collision into account. The "$\exp\left(\frac{E_a}{R_u T}\right)$" term derives from the Maxwell–Boltzmann distribution of molecular speeds and is proportional to the fraction of atoms or molecules that have a kinetic energy greater than the *activation energy* E_a that is required for a collision to initiate reaction. The values of A, E_a, and the temperature exponent n are usually derived from experimental measurements of reaction rate.

Most elementary reactions are bimolecular, as in this generic example. It is common in combustion applications to approximate the detailed chemical reactions with a global reaction rate (e.g., $CH_4 + 2O_2 \rightarrow CO_2 + 2H_2O$). Even in this case, the Arrhenius form is still used, although the constants A, E_a, and n are now fitting coefficients that may have a limited range of validity.

Usually, it is also necessary to consider the backward reaction as well (i.e., reversible reactions): C + D → A + B. However, the reaction rate constants in this case can be expressed in terms of the equilibrium constant as follows. At equilibrium (A + B ⇌ C + D), the rate of forward and backward reactions must be equal, such that the overall composition remains constant. Thus,

$$C_{\mathrm{A}} C_{\mathrm{B}} k_{\mathrm{f}} = C_{\mathrm{C}} C_{\mathrm{D}} k_{\mathrm{b}} \tag{2.63}$$

$$\frac{k_{\mathrm{f}}}{k_{\mathrm{b}}} = \frac{C_{\mathrm{C}} C_{\mathrm{D}}}{C_{\mathrm{A}} C_{\mathrm{B}}} = K_c, \tag{2.64}$$

where K_c is the equilibrium constant based on concentration. If the stoichiometric coefficients are other than unity (e.g., $\nu_{\mathrm{A}}\mathrm{A} + \nu_{\mathrm{B}}\mathrm{B} \rightarrow \nu_{\mathrm{C}}\mathrm{C} + \nu_{\mathrm{D}}\mathrm{D}$), then

$$\frac{k_{\mathrm{f}}}{k_{\mathrm{b}}} = \frac{C_{\mathrm{C}}^{\nu_{\mathrm{C}}} C_{\mathrm{D}}^{\nu_{\mathrm{D}}}}{C_{\mathrm{A}}^{\nu_{\mathrm{A}}} C_{\mathrm{B}}^{\nu_{\mathrm{B}}}} = K_c. \tag{2.65}$$

The equilibrium constant based on partial pressure K_p is related to the equilibrium constant based on concentrations K_c as follows:

$$K_p = \frac{\left(\frac{p_{\mathrm{C}}}{p_{\mathrm{ref}}}\right)^{\nu_{\mathrm{C}}} \left(\frac{p_{\mathrm{D}}}{p_{\mathrm{ref}}}\right)^{\nu_{\mathrm{D}}}}{\left(\frac{p_{\mathrm{A}}}{p_{\mathrm{ref}}}\right)^{\nu_{\mathrm{A}}} \left(\frac{p_{\mathrm{B}}}{p_{\mathrm{ref}}}\right)^{\nu_{\mathrm{B}}}} = K_c \left(\frac{R_u T}{p_{\mathrm{ref}}}\right)^{(\nu_{\mathrm{C}}+\nu_{\mathrm{D}}-\nu_{\mathrm{A}}-\nu_{\mathrm{B}})}, \tag{2.66}$$

where p_{ref} is the reference pressure used in defining the equilibrium constant based on partial pressures.

Equilibrium constants are derived from thermodynamic data as follows:

$$K_p = \exp\left(-\frac{\nu_{\text{C}}\bar{g}^{\circ}_{\text{fC}} + \nu_{\text{D}}\bar{g}^{\circ}_{\text{fD}} - \nu_{\text{A}}\bar{g}^{\circ}_{\text{fA}} - \nu_{\text{B}}\bar{g}^{\circ}_{\text{fB}}}{R_u T}\right), \tag{2.67}$$

where $\bar{g}^{\circ}_{\text{f}}$ is the Gibbs function on a per mole basis of species i evaluated at the temperature T and at the reference pressure $p_{\text{ref}} = 1\,\text{atm}$. Thus, the equilibrium constants, in being derived from fundamental thermodynamic data, are known with much greater confidence than kinetic rate constants. This approach then ensures that the overall kinetic mechanism is consistent with the higher-confidence equilibrium constants. A consequence of this assumption is that it is possible to start with a completely arbitrary or incorrect reaction mechanism and still reach the correct equilibrium composition of a reacting gas mixture. Thus, correctly reproducing the CJ detonation velocity via a ZND calculation with detailed chemistry should not be taken as validation of the kinetic mechanism.

The overall conversion of fuel and oxidizer into products is described by a kinetic mechanism, consisting of elementary reactions. For most combustible mixtures, it is necessary to consider numerous possible reactions. Even a "simple" system like hydrogen/oxygen is typically modeled with 20 or so elementary reactions, while mechanisms for hydrocarbon fuels (e.g., methane) can consider reactions numbering in the hundreds or thousands.

For a mechanism consisting of $j = 1, 2, \ldots, M$ elementary reactions that describes the reaction of $i = 1, 2, \ldots, N$ species, the overall production rate of species i is given by

$$\dot{\omega}_i = \sum_{j=1}^{M} \nu_{ij} r_j \tag{2.68}$$

$$r_j = k_{\text{f}_j} \prod_{i=1}^{N} C_i^{\nu'_{ij}} - k_{\text{b}_j} \prod_{i=1}^{N} C_i^{\nu''_{ij}}, \tag{2.69}$$

where ν'_{ij} is the stoichiometric coefficient of species i in the forward reaction j and ν''_{ij} is the corresponding stoichiometric coefficient for the backward reaction. If a species is absent from a reaction, its stoichiometric coefficient is zero.

The time rate of change of concentration is often expressed in the combustion literature as

$$\frac{\text{d}C_i}{\text{d}t} = \dot{\omega}_i. \tag{2.70}$$

This expression is strictly only valid for a constant volume (density) reaction. In general, reacting flows are variable density, so species concentrations can change due to changes in density as well as reaction, and thus (2.70) is

not valid. This point is rarely expressed in most combustion textbooks, with [87] being a notable exception. For this reason, when working with reactive compressible flows, it is preferable to express species concentration in terms of mass fraction using $C_i = \frac{\rho Y_i}{W_i}$. The rate of change of mass fraction is then given by

$$\mathrm{d}Y_i = \frac{\dot{\omega}_i}{\rho u}. \tag{2.71}$$

The one caveat that must be issued in regards to numerical integration of the reaction zone structure is that chemical kinetic mechanisms tend to be numerically *stiff*. Stiffness in this context refers to the fact that the timescales of different processes occurring in a simulation (in this case, different chemical reactions) can vary greatly, often by many orders of magnitude. For example, it is possible for a chemical species that is not initially present to appear suddenly during the evolution of a reaction due to a chain-branching mechanism, only to be quickly consumed again. If too large of a numerical time step is taken, this feature may be missed or introduce numerical instability into the solution. The enormous computational power of today's computers may make it tempting to simply use a very small time step for the entire numerical integration; however, this approach can lead to the accumulation of numerical error, affecting the solution as well. The best approach is to use a numerical method that senses regions of the solution where a property is varying rapidly and decreases the numerical step size accordingly (e.g., predictor/corrector methods). Fortunately, most current high-level numerical packages have built-in ODE solvers that are designed to handle stiff systems of equations; [62] can be consulted for more details regarding implementing numerical methods for stiff reactive systems.

2.5.2 Carbon Monoxide/Oxygen System

As a sample calculation, the one-dimensional steady structure of a carbon monoxide/oxygen detonation will be computed. This system has the advantage that it is described by a very simple mechanism consisting of just three reactions considering four species:

$$\mathrm{CO} + \mathrm{O} + \mathrm{M} \rightleftharpoons \mathrm{CO_2} + \mathrm{M} \tag{2.72}$$

$$\mathrm{CO} + \mathrm{O_2} \rightleftharpoons \mathrm{CO_2} + \mathrm{O} \tag{2.73}$$

$$\mathrm{O} + \mathrm{O} + \mathrm{M} \rightleftharpoons \mathrm{O_2} + \mathrm{M}. \tag{2.74}$$

Here M is a generic third body (i.e., M can be CO, O_2, CO_2, or O). The values of the reaction rate constants are given in Table 2.1. Experimentally, this system is not very easy to realize (beyond the toxicity of carbon monoxide) due to the high activation energy of the $\mathrm{CO} + \mathrm{O_2} \rightleftharpoons \mathrm{CO_2} + \mathrm{O}$ reaction. In the presence of even trace amounts of hydrogen, OH molecules can form and then promote the formation of CO_2 more readily via the reaction $\mathrm{CO} + \mathrm{OH} \rightleftharpoons \mathrm{CO_2} + \mathrm{H}$. The H is then "recycled" back into OH, resulting in a catalytic-like

Table 2.1. Carbon monoxide/oxygen reaction mechanism

Reaction	A	n	E_a (kJ/kmol)
$CO + O + M \rightleftharpoons CO_2 + M$	1.8×10^{4a}	0.00	9,970
$CO + O_2 \rightleftharpoons CO_2 + O$	2.5×10^{9b}	0.00	200,000
$O + O + M \rightleftharpoons O_2 + M$	1.2×10^{11a}	−1.00	0

[a] $m^6 kmol^{-2} s^{-1}$
[b] $m^3 kmol^{-1} s^{-1}$

role of hydrogen in converting the CO into CO_2. Thus, in any real system with even trace contamination of hydrogen, water, or hydrocarbons, the mechanism (2.72)–(2.74) is not the dominant reaction path. For the purposes of a model system to explore numerically, however, the dry oxidation of carbon monoxide is convenient to use.

In order to initialize the calculation of the reaction zone structure at the von Neumann point, it is necessary to specify the propagation velocity of the detonation wave. This was done in two different ways: an *equilibrium solution* based on a control volume enclosing the wave and a *ZND solution* in which the structure of the reaction zone is solved. The equilibrium solution based on a control volume was determined through iteration upon the integral conservation laws (2.1)–(2.3) assuming chemical equilibrium at the exit plane until the minimum wave velocity solution was found. The reaction zone structure was not considered in this case. The speed of sound was not explicitly introduced in these calculations, but the solution found corresponds to sonic outflow (i.e., flow velocity equals the equilibrium speed of sound). This solution methodology can be shown to agree with that used in well-known equilibrium programs such as the NASA CEA program [34,56], and generates the same results within numerical precision.

The ZND-based solution was found by numerically integrating the reaction zone structure using the (2.58)–(2.71). The initial velocity of the wave was iterated upon until a solution that had sonic outflow and that did not encounter a singularity was found. Note that the sonic outflow condition found is that defined by using the equilibrium speed of sound. The outflow with respect to the frozen speed of sound was still subsonic (Mach 0.963). Therefore, this solution does not satisfy the generalized CJ condition (2.59).

The results of the two solution methodologies are compared in Table 2.2. The propagation velocity of the detonation wave found by these two methods agrees to six significant digits, and the flow properties at the exit state agree to within five or six significant digits. Thus, it can be concluded that these two methods find the same solution for the detonation wave.

The structure of the wave is shown in Fig. 2.10. The reaction zone length, as defined by identifying the location of maximum thermicity or the inflection point in temperature, is on the order of 10–15 cm. However, the sonic condition (using the equilibrium sound speed) is only approached asymptotically. Thus,

Table 2.2. Carbon monoxide/oxygen detonation

Initial composition	(moles)	$CO + \frac{1}{2}O_2$	
	p_1 (kPa)	101.325	
Initial state	T_1 (K)	300.000	
	c_1 ($m\,s^{-1}$)	344.705	
Detonation solution		Equilibrium	ZND
	u_1 ($m\,s^{-1}$)	1,798.32	1,798.32
	M_{1_f}	5.21698	5.21698
	p_{vN} (kPa)	3,288.67	3,288.67
	p_{vN}/p_1	32.4566	32.4566
	T_{vN} (K)	1,684.98	1,684.98
von Neumann state	u_{vN} ($m\,s^{-1}$)	311.198	311.198
	c_{vN} ($m\,s^{-1}$)	787.579	787.579
	M_{vN}	0.395132	0.395132
	p_2 (kPa)	1,861.26	1,861.28
	p_2/p_1	18.3692	18.3694
	T_2 (K)	3,523.31	3,523.31
Chapman–Jouguet	u_2 ($m\,s^{-1}$)	977.182	977.177
state	c_{f_2} ($m\,s^{-1}$)	1,014.43	1,014.43
	c_{e_2} ($m\,s^{-1}$)	977.183	977.183
	M_{f_2}	0.96329	0.96328
	M_{e_2}	1.00000	0.99999

it is not possible to define a hydrodynamic thickness of the wave based of the location of the sonic surface (or, any definition of the total thickness of the wave using the flow Mach number—such as where the flow reaches Mach 0.99 for example—would be arbitrary).

It is of interest to explore if an eigenvalue solution for this problem can be found that does satisfy the generalized CJ solution, in contrast to the equilibrium solution found above. Recall that the equilibrium solution has subsonic outflow (Mach 0.963) with respect to the frozen speed of sound. In order to have the exit flow reach sonic with respect to the frozen speed of sound, it is necessary to decrease the wave speed, thus increasing the post-shock flow velocity and thereby making it possible for the heat release of reaction to bring the flow to frozen sonic velocity c_f. However, if the initial velocity of the wave in the equilibrium solution found above is decreased by just $0.1\,m\,s^{-1}$, the solution for reaction zone structure encounters a singularity, as shown in Fig. 2.11. The flow velocity reaches the frozen sound speed at $x \approx 1\,m$, but the thermicity has a positive (nonzero) value that prevents the solution from passing through a saddle point. Decreasing the wave velocity further results in this singularity occurring earlier in the flow. Increasing the wave velocity by $0.1\,m\,s^{-1}$ above the CJ solution results in the flow remaining subsonic with respect to both the frozen and equilibrium sound speeds (i.e., strong detonation solution). Thus, no eigenvalue solution to the wave structure

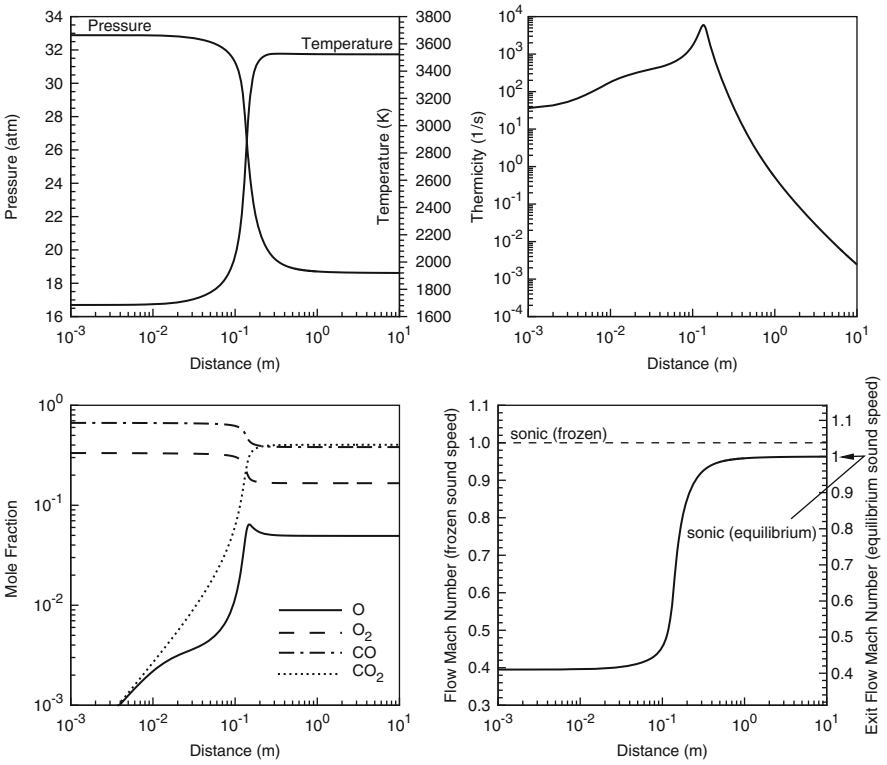

Fig. 2.10. Structure of CO/O_2 detonation, showing pressure, temperature, mole fractions, thermicity, and flow Mach number. Note that Mach number is plotted using the local, frozen speed of sound on the left y-axis, the right y-axis gives the exit flow Mach number using the equilibrium speed of sound

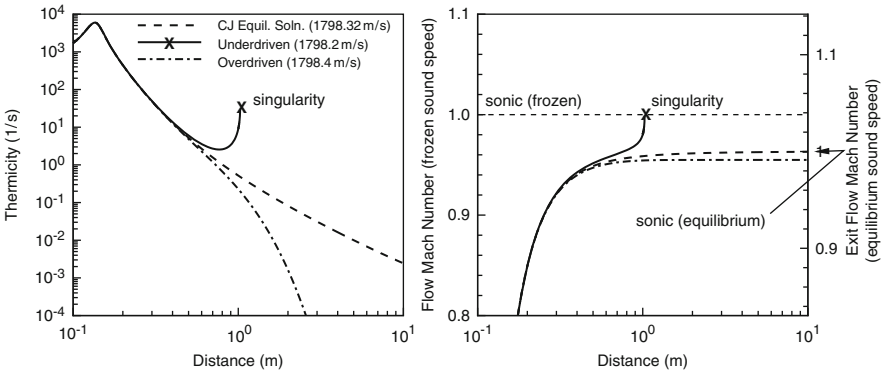

Fig. 2.11. Structure of CO/O_2 detonation, initialized with a velocity slightly above and slightly below the equilibrium CJ solution

exists in this case that permits the solution to satisfy the generalized CJ criterion. This result is due to the fact that the thermicity parameter is always positive and only approaches zero asymptotically. In order for the solution to pass through sonic via a saddle point, the thermicity must pass through zero. Thus, for the carbon monoxide/oxygen system discussed here, there is no ambiguity since the equilibrium and the ZND-based methods generate the same unique solution.

2.5.3 Hydrogen/Chlorine System

Identification of a real combustible mixture that exhibits the type of pathological behavior discussed in Sect. 2.3 is an interesting problem that has been the subject of periodic investigation since the introduction of the ZND model in the 1940s. Zeldovich and Ratner [108] pointed out that the reaction of H_2 and Cl_2 to form HCl can occur via the Nernst chain reaction much more readily than the dissociation of Cl_2, which has a relatively high activation energy. Thus, the highly exothermic reaction forming HCl may be followed by an endothermic dissociation reaction in Cl_2, resulting in the type of exothermic/endothermic reaction necessary for pathological behavior. Subsequent studies of experimental systems exhibiting pathological behavior have tended to focus on this system.

The first detailed chemical kinetic calculations of a ZND detonation in H_2/Cl_2 were performed by Guénoche et al. [37] using the mechanism given in Table 2.3. These calculations are reproduced here. A fuel-lean (chlorine-rich) mixture with fuel equivalence ratio $\phi = 0.66$ at relatively low pressure ($p_1 = 3.33\,\text{kPa}$) was selected here for a sample calculation in order to accentuate the difference between the rapid, exothermic formation of HCl and the slower dissociation of the excess Cl_2. The governing differential equations (2.58)–(2.71) were integrated coupled with the kinetic mechanism in Table 2.3. The initial shock velocity was iterated upon until a solution that

Table 2.3. Hydrogen/chlorine reaction mechanism

Reaction	A ($\text{m}^3\text{kmol}^{-1}\text{s}^{-1}$)	n	E_a (kJ/kmol)	M
$H + H + M \rightleftharpoons H_2 + M$	1.0×10^{12}[a]	−1.00	0	HCl, Cl_2, Cl
	2.0×10^{13}[a]	−1.00	0	H
	2.0×10^{10}[a]	−0.60	0	H_2
$Cl_2 + M \rightleftharpoons 2Cl + M$	6.15×10^{18}	−2.07	238,815	H_2, Cl_2, HCl, H
	6.15×10^{19}	−2.07	238,857	Cl
$HCl + M \rightleftharpoons H + Cl + M$	6.76×10^{18}	−2.00	427,765	H_2, Cl_2, HCl, H, Cl
$Cl + H_2 \rightleftharpoons HCl + H$	4.80×10^{10}	0.00	22,023	
$H + Cl_2 \rightleftharpoons HCl + Cl$	6.61×10^{8}	0.68	4,564	

[a] $\text{m}^6\text{kmol}^{-2}\,\text{s}^{-1}$

Table 2.4. Hydrogen/chlorine detonation

Initial composition	(Moles)	$H_2 + \frac{3}{2}Cl_2$	
	p_1 (kPa)	3.33	
Initial state	T_1 (K)	300.00	
	c_1 ($m\,s^{-1}$)	278.93	
Detonation solution		Equilibrium	Eigenvalue (ZND)
	u_1 ($m\,s^{-1}$)	1,320.7	1,527.3
	M_{1_f}	4.735	5.476
von Neumann state	p_{vN} (kPa)	86.469	116.06
	p_{vN}/p_1	18.066	34.852
	T_{vN} (K)	1,374.1	1,724.4
	u_{vN} ($m\,s^{-1}$)	232.96	251.88
	c_{vN} ($m\,s^{-1}$)	586.81	655.23
	M_{vN}	0.3970	0.3844
Chapman–Jouguet state	p_2 (kPa)	47.073	60.300
	p_2/p_1	14.136	18.108
	T_2 (K)	2,075.94	2,989.09
	u_2 ($m\,s^{-1}$)	748.4	883.3
	c_{f_2} ($m\,s^{-1}$)	789.0	883.3
	c_{e_2} ($m\,s^{-1}$)	748.4	N/A
	M_{f_2}	0.9485	1.0000
	M_{e_2}	1.0000	N/A

passes through the frozen sonic point was identified. This solution is presented in Table 2.4 and Fig. 2.12, showing the thermodynamic properties, species concentrations, thermicity parameter, and the flow Mach number (using the frozen speed of sound). As hypothesized by Zeldovich and Ratner, the H_2/Cl_2 system does exhibit an overshoot in the heat release followed by an endothermic phase. This is most clearly seen by examining the temperature and the thermicity parameter, which passes through zero and becomes negative at the same point where the flow becomes frozen sonic, as required by the generalized CJ condition. (Note the fact that the thermicity becomes negative prevents the use of a log-scale on the y-axis, in comparison to Fig. 2.10.) The history of species concentrations through the reaction zone verifies that the rapid formation of HCl followed by a slower dissociation of Cl_2 into Cl is the source of the exothermic/endothermic nature of the reaction. This solution, resulting from iteration upon the reaction zone structure until a trajectory that satisfies the generalized CJ condition was found, is the eigenvalue solution.

The eigenvalue solution found above is compared to the equilibrium solution, such as would be found via the NASA CEA [34, 56] or other chemical equilibrium software, in Table 2.4. A significant difference between the two solutions is found, with a 15% discrepancy in the detonation propagation velocities with the equilibrium velocity being lower. This result is unlike that

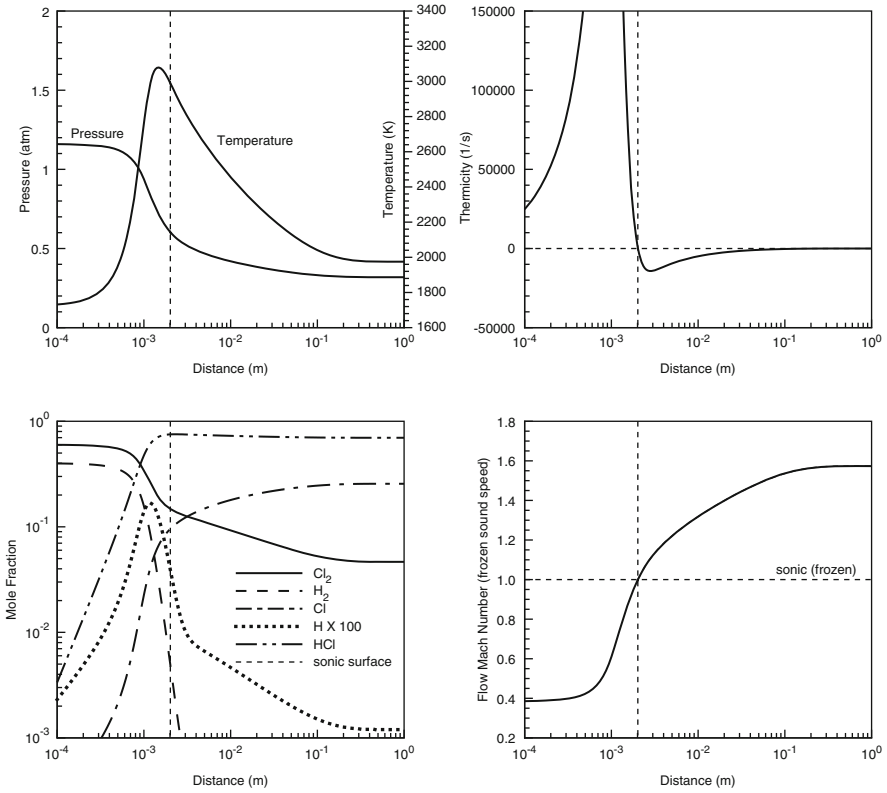

Fig. 2.12. Structure of H_2/Cl_2 detonation, showing pressure, temperature, mole fractions, thermicity, and flow Mach number. The location of the sonic point is denoted as a *vertical dashed line*

obtained with CO/O_2 detonations considered in the prior section, for which the equilibrium and ZND approaches were seen to generate the same solution (within numerical precision). If a ZND calculation of the H_2/Cl_2 reaction zone is initialized with the post-shock von Neumann conditions for the CJ equilibrium solution, as is done in Fig. 2.13, the calculation encounters a singularity. The reaction zone is now longer due to the lower post-shock temperature, but when the exothermic reaction begins to release significant heat into the flow, it results in sonic flow being encountered before the thermicity going to zero, hence causing the singularity. Qualitatively, this is identical to the behavior seen in Sect. 2.3 with an artificially constructed two-step endothermic/exothermic system. Indeed, any attempt to initialize a solution with a shock velocity even incrementally below the eigenvalue solution for the H_2/Cl_2 system results in a singularity. Solutions initialized with a faster shock remain subsonic with respect to the frozen speed of sound (i.e., the strong detonation solution). Finally, note that it is not possible to define an equilibrium sound speed for the (nonequilibrium) sonic point of the eigenvalue solution.

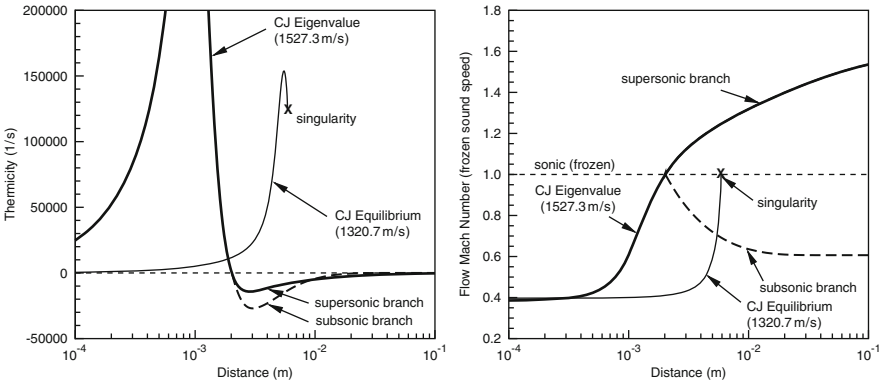

Fig. 2.13. Structure of H_2/Cl_2 ($\phi = 0.666, p_1 = 3.33\,\text{kPa}$) detonation, initialized with CJ equilibrium (resulting in a singularity) and eigenvalue solutions. Both the supersonic and subsonic downstream branches of the eigenvalue solution are shown

The experimental realization of this pathological behavior in the H_2/Cl_2 system has been attempted several times, starting with Zeldovich and Ratner [108], followed by [1, 46]. Comparing these different experiments indicates some inconsistent results, likely due to initiation transients or unstable waves caused by finite tube size effects. While measurement of detonation velocity is conceptually very easy (consisting of just recording the time of arrival at two spatially separated locations), in practice great care must be exercised that the measured propagation velocity is not influenced by the initiation mechanism or near-limit effects due to using too small a detonation tube. The most recent and careful study is that of Dionne et al. [21], who used a long (12-m-long) tube with 5-cm inside diameter. The final 8 m of tube was instrumented with four pressure sensors to verify that a stable detonation wave had been initiated by the powerful spark used. The results of measurements of the detonation propagation velocity are shown in Fig. 2.14, giving the wave velocity as a function of initial pressure for a fuel lean mixture ($\phi = 0.66$). Also shown are the detonation velocity as predicted by the CJ equilibrium solution and the eigenvalue solution as calculated via iteration upon the ZND structure. Note that the velocity of the eigenvalue solution exhibits a very nearly flat dependence on pressure, due to the fact that it only depends upon the exothermic phase of HCl formation and independent of the subsequent dissociation, which is isolated from the front via the sonic point. The equilibrium solution shows a gradual decrease in velocity due to the increased dissociation at lower pressure resulting in less complete combustion and thus less total heat release. This equilibrium behavior is typical of most mixtures.

The experimental data appear to match the equilibrium solution at higher pressure, but as the pressure is decreased, the observed detonation velocities remains constant or slightly increases, moving away from the equilibrium solution and toward the eigenvalue solution. This pressure independence of

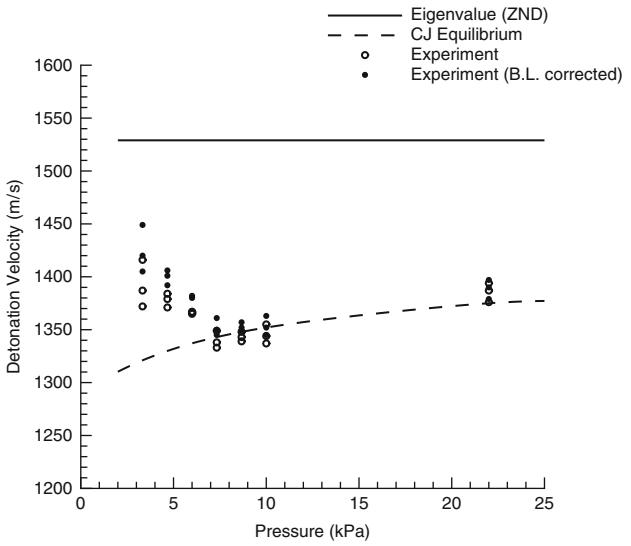

Fig. 2.14. Comparison of experimental measurements of detonation velocities in H_2/Cl_2 ($\phi = 0.66$), CJ equilibrium, and eigenvalue (ZND-based) solutions. Experimental data are shown as *open symbols*, velocities corrected for boundary layer effects are shown as *solid symbols*

H_2/Cl_2 detonation velocity was first experimentally noted in 1934 by Sokolik and Shchelkin [82]. In actuality, the experimental detonation velocity would be expected to decrease as pressure is decreased, even if the experimental detonations correspond to the eigenvalue solution, since the longer reaction zone at lower pressure should experience increased losses associated with the tube walls. For this reason, Dionne et al. corrected their experimental data, extrapolating the measured velocities to what would be expected in an effectively infinite diameter tube (i.e., the ideal CJ velocity) by using the Fay–Dabora model [18,28]. These corrected data are also shown in Fig. 2.14 and moves the data toward the predictions of the eigenvalue solution, particularly at lower pressures. Note that the largest deviation from the equilibrium solution occurs at $p_1 = 3.33\,\text{kPa}$ (the experimental result being about 10% greater than the equilibrium solution), which is why this condition was selected for the sample calculations shown in Figs. 2.12 and 2.13. Dionne et al. also studied mixtures at stoichiometric ($\phi = 1$) and rich ($\phi = 1.5$) equivalence ratios as well, which also exhibited pathological behavior, although to a lesser degree [21].

While the results with H_2/Cl_2 are not as convincing a demonstration of a pathological detonation as might be hoped, some discussion of the comparison between experiment and theory in Fig. 2.14 is in order. For perspective, experimentally observed detonation velocities are usually 1–2% below the equilibrium solution, provided care has been exercised to isolate the initiation transients and near-limit effects discussed above, so the discrepancy of an

observed velocity 10% greater than the equilibrium velocity is experimentally significant. In addition, the ZND model neglects the fact that the detonation zone structure is influenced by the unsteady longitudinal pulsations and transverse wave interactions that comprise the cellular structure of the shock front, as is the case in all known detonable mixtures including H_2/Cl_2. Finally, the chemical kinetics model used (Table 2.3) is relatively primitive, dating from the 1970s, and likely should be updated to include vibrationally excited states, as discussed in [91].

Future investigations of pathological behavior deriving from systems with exothermic/endothermic behavior might also consider gaseous hydrogen azide (HN_3), which has been observed to support detonation propagation velocities approximately 7.5% greater than the CJ equilibrium solution [63]. A further recommendation to future studies would be to focus on measurement of properties such as pressure or temperature, which, while being a greater diagnostic challenge, are much more sensitive to the differences in detonation solution (equilibrium versus eigenvalue), as can be seen from Table 2.4. Detonation velocity, which has only a square root dependence on energy release ($D_{CJ} \sim \sqrt{Q}$), is a comparatively insensitive parameter. Another intriguing possibility to realize a pathological detonation is a system that exhibits a large molar decrement. Returning to (2.58), note that the thermicity (numerator) can be brought to zero via an increasing molecular weight (rather than, or in combination with, endothermic reactions). In other words, a mixture that reacts to produce a product composition with fewer moles than the reactants may also exhibit pathological behavior. In pure gaseous systems, this condition is difficult to realize, since the elevated temperatures of reaction result in dissociation and low molecular weight products in comparison to the reactants. However, two-phase reactive systems (e.g., a solid fuel in a gaseous oxidizer) exist that might bring about this condition. Many metals (aluminum, magnesium, zirconium) have refractory oxidation products that should remain largely in the condensed phase even at adiabatic flame temperatures, resulting in a system exhibiting a large molar decrement. The use of a two-phase system introduces a number of additional complexities that might further challenge the interpretation of the results, such as a lack of mechanical or thermal equilibrium between the phases; two-phase detonations are discussed further in [111,112]. Finally, it is likely that many condensed-phase detonations have late endothermic phases to their reaction mechanisms, making them also candidates for pathological behavior. A recognizable example is an emulsion-based blasting compound with large "prills" of ammonium nitrate or large, reactive metal particulates that are only intended to react to completion during the expansion of the post-detonation products [30]; such a system almost certainly exhibits pathological behavior in comparison to solutions that assume complete equilibrium at the sonic point. The large uncertainties in the product equations of state (necessary for accurate equilibrium calculations) and a lack of equilibration between phases, however, make unambiguous identification of deviations from the equilibrium solution difficult for condensed-phase

explosives. For a further, contrasting assessment of the likelihood of pathological detonations, see [91].

2.5.4 Frozen and Equilibrium Sound Speed

An issue that arises in the application of the CJ criterion and its generalization to nonideal detonations is which sound speed should be used in defining the sonic condition. In a chemically reacting flow, there are two limits to sound wave propagation, namely frozen and equilibrium. The frozen sound speed corresponds to the case of a very high-frequency sound wave (or, alternatively, very slow reactions) where the mixture does not have time to react over the duration of the acoustic wave and the mixture composition remains fixed. The equilibrium sound speed applies for very low frequency sound (or, very fast reactions) in which case the mixture can react quickly enough to remain in chemical equilibrium throughout the isentropic compression or rarefaction pulse that comprises the acoustic wave. It can be shown that the frozen speed of sound is always greater than the equilibrium speed of sound [19]. In real reacting gases, sound waves propagate in between these two limiting speeds, which are typically about 5% different in combustion products. The issue of which sound speed should be used in applying the CJ criterion was discussed intensively in the 1950s and was never satisfactorily resolved [10,24,36,44,102–104]. In addition to detonations, the issue of which sound speed to use in defining the flow regime arises in other nonequilibrium reactive flows as well, such as in hypersonics [4, 99].

To explore this issue, consider a planar detonation in the absence of losses and having a positive thermicity that proceeds asymptotically toward equilibrium. When solving for the ZND structure, the integration proceeds down the Rayleigh line from the von Neumann point and reaches the same equilibrium sonic point that is found by applying the classical CJ condition to the equilibrium Hugoniot. In this case, as was found with the carbon monoxide/oxygen system considered in Sect. 2.5.2, there is no conflict between the classical CJ condition and the ZND-based solution. Viewed on the (p, v) plane, detonations at sub-CJ velocities do not reach the equilibrium Hugoniot and thus no steady solution can be obtained (this is the scenario wherein a singularity appears), while detonations traveling faster than the CJ equilibrium solution will have a reaction zone trajectory that proceeds down the Rayleigh line and stops when it intersects the equilibrium Hugoniot at the upper intersection point (strong detonation with subsonic flow). Thus, the CJ equilibrium solution is the only steady solution to feature a sonic point, and that sonic point is defined by the equilibrium sound speed.

Since the CJ solution in this case has equilibrium sonic outflow, the flow through the entire reaction zone remains subsonic in comparison to the frozen speed of sound (see Table 2.2), and it could be argued that such a solution would be susceptible to high frequency rarefactions catching up to the

wave from behind and disrupting the reaction zone. However, as a detonation propagates, the gradient of expansion behind the wave becomes more gradual, and thus the frequency of rarefaction waves might be expected to approach the low (equilibrium) limit. Further, while the initial leading edge of a centered rarefaction would propagate at the frozen speed of sound, this acoustic wave is quickly attenuated (decays exponentially) and the majority of the rarefaction is governed by the equilibrium speed of sound. This aspect of rarefactions propagating in reactive flow was explored in detail by Wood and Parker [103]. If this is the case, then the equilibrium solution would agree with the conceptual picture of the CJ detonation being isolated from downstream disturbances by a sonic plane.

For a system with pathological heat release, such as the hydrogen/chlorine system considered in Sect. 2.5.3, it is not possible to obtain a solution for the reaction zone structure that is initialized with the CJ equilibrium value of detonation speed (see Fig. 2.13). This case can be visualized on the (p, v) plane by the inability of a sequence of intermediate Hugoniots to provide a path along the Rayleigh line to a state of tangency to the equilibrium Hugoniot (see Fig. 2.5). The only permitted steady solution with a sonic point is the eigenvalue solution with a frozen sonic point embedded in the solution and an exit flow that, with respect to the equilibrium Hugoniot, is a weak detonation. Similarly, in any system with losses such as heat transfer or friction, as discussed in Sect. 2.4 or with laterally divergent flow, as will be discussed in Sect. 2.6, it is the frozen sound speed that defines the saddle point of the eigenvalue solution.

This situation gives rise to an apparent paradox, wherein the limiting solution as the loss mechanism decreases to zero may not converge to the ideal, planar solution, since the former is defined by the frozen speed of sound and the latter uses the equilibrium speed of sound. For example, for the case of a detonation in a tube with losses at the walls, as the radius of the tube increases to infinity, the solution for the detonation velocity will not agree with the planar solution (i.e., $\lim_{r\to\infty} D \neq D_{r=\infty}$). In order to resolve this apparent inconsistency, a possible strategy would be to solve the full, unsteady Euler equations without imposing a particular criterion, and see which solution evolves (this approach was done by Sharpe and Falle [75, 77] for pathological detonations and by Dionne et al. [22] for detonations with friction and heat transfer, as discussed in Sect. 2.4.3). Such a calculation was performed by Sharpe [76] for a model system with a single-step reversible chemistry originally proposed by Fickett and Davis [19] (Fickett and Davis considered a system with zero activation energy, while Sharpe considered a system with low activation energy that gave a stable ZND solution). Sharpe [76] showed that, for a planar detonation initiated by an overdriven blast wave in the above system, after a long propagation time, the wave velocity and reaction zone structure approached that of an equilibrium sonic CJ detonation. However, if even an infinitesimal degree of loss was introduced (curvature, in the case of Sharpe's calculations), the long-term evolution of the solution converged

toward the eigenvalue solution with a frozen sonic point where thermicity went to zero (note that Sharpe included the effect of area divergence into his definition of thermicity). Thus, it appears that the counterintuitive scenario discussed above, where the solution in the limit of losses going to zero does not converge to the ideal CJ equilibrium solution, is indeed the case.

Since all real detonations are multidimensional and transient, making the definition of a sonic point or plane in the flow problematic, the equilibrium versus frozen sound speed issue is now regarded as being somewhat academic. The issue does occasionally arise in connection with the hydrogen/oxygen system (or hydrogen/air), which was speculated by Fickett and Davis [19] to exhibit pathological behavior due to molar decrement. Differences between the CJ equilibrium solution and a solution obtained by iterating upon a ZND calculation for hydrogen/air were found by Klein et al. [45] and attributed to the comparatively slow, endothermic dissociation of water resulting in slightly negative values of thermicity at the end of the reaction zone. In this case, the solution is of the eigenvalue type with a frozen sonic point. Discrepancies between ZND and CJ equilibrium solutions for hydrogen/oxygen were also noted by [67] but not explored further. Hydrogen/oxygen was not selected as a sample reactive system in this chapter for precisely this reason, namely, that it may exhibit weakly pathological behavior depending upon the details of the particular kinetics mechanism used.

2.6 Detonations with Divergent Flow

Detonation waves (both condensed-phase and gaseous) propagating in finite-sized charges will be subject to losses resulting from divergent flow at the periphery of the charge. The pressures within the reaction zone of any condensed-phase detonation (typically, 10–30 GPa) greatly exceed the yield strength of any confining material, resulting in an outward expansion of the detonation products as the confinement gives way. The loss in axially directed momentum in the flow of detonation products causes the detonation to propagate at a slower velocity than would be obtained in a rigidly confined charge or, equivalently, in a planar detonation in an infinite-sized charge (i.e., an infinite-sized charge is "self-confined" and is expected to detonate at the ideal CJ velocity). The lower propagation velocity additionally lowers the post-shock temperature/pressure and consequently the chemical reaction rates, while the diverging flow can cause the sonic surface to occur earlier in the reaction zone, such that less energy release is available to drive the detonation wave. The divergent flow also necessitates that the leading shock front is no longer planar and becomes curved. These effects become progressively more significant as the dimension of the charge is decreased until eventually the detonation wave fails altogether. With condensed-phase explosives, this failure process can be spectacularly abrupt; it is not uncommon to recover nearly pristine, unreacted explosive only one charge diameter beyond the point at

which the critical dimension is first encountered. In gaseous explosives contained in rigid tubes, near-limit behavior is more complex, since the wave can interact with the tube wall in order to sustain propagation in transient modes known as spinning and galloping detonations (see discussion in Chap. 7 of [51]).

The velocity deficit in finite-sized charges and the existence of a critical dimension (usually, the diameter of a cylindrical charge) are heavily utilized in research on detonation waves in condensed-phase explosives as a means to probe the reaction zone structure and thermodynamic properties of the detonation products. Due to the extremely short reaction timescales in condensed-phase detonations (typically, sub-microsecond to nanosecond), the opaque nature of detonating media, and the extreme pressures generated, in situ measurements of any detonation properties are extraordinarily difficult. As a result, almost all models for condensed-phased detonations utilize data derived from the velocity deficit and/or the curvature of the shock front as the charge diameter is decreased, or measurement of the critical diameter at which detonation failure occurs. The radial expansion of detonation products in a cylindrical charge confined with a ductile material (e.g., copper) is also the basis of most semi-empirical models for the equation of state of the detonation products.

For detonations in gas-phase media on the order of atmospheric pressure, perfectly rigid confinement is possible, for example, using a steel-walled tube. However, the periphery of the gaseous charge still influences the detonation wave via friction and heat transfer to the wall. In Sect. 2.4, these effects were treated as volumetric losses that were spread uniformly across the cross section of the tube. In reality, the influence of the wall is conveyed to the detonation flow via a boundary layer region near the wall. The growth of the boundary layer results in a diverging flow in the reaction zone, qualitatively similar to the diverging flow that occurs in a condensed-phase detonation due to yielding confinement. It may appear counterintuitive that growth of a boundary layer along the wall results in a *diverging* flow in the detonation reaction zone; note that in the wave-fixed reference frame, the walls have the effect of accelerating the flow while also cooling and increasing the density of gas in the boundary layer. By continuity, this effect requires that the core of the flow diverges outward to account for the mass effectively removed by the boundary layer. Boundary layers of this type are sometimes called *negative boundary layers*. Within the context of a quasi-one-dimensional approximation, detonations with divergent flow can be treated with the reaction zone equations derived previously in Sect. 2.2. In particular, (2.10), reproduced here slightly modified

$$\frac{\mathrm{d}u}{\mathrm{d}x} = \frac{\frac{\Delta q}{c_p T}\dot{\lambda} - u\frac{1}{A}\frac{\mathrm{d}A}{\mathrm{d}x}}{1 - M^2}, \tag{2.75}$$

models the effect of diverging flow via the $\frac{1}{A}\frac{\mathrm{d}A}{\mathrm{d}x}$ term. In this section, the steady reaction zone structure of detonation waves with diverging flow is further

explored with a particular emphasis on models that permit the area divergence term to be quantified.

2.6.1 Stream Tube Divergence

If the stream tube defining the reactive flow in the detonation is a two-dimensional slab with yielding confinement on the top and bottom surfaces only or an axisymmetric cylindrical tube with yielding confinement on the circumference, the area of the stream tube is given by

$$\text{2-D Slab:} \quad A(x) = t(x)\, w \tag{2.76}$$

$$\text{Axisymmetric Tube:} \quad A(x) = \frac{1}{4}\pi d(x)^2 \tag{2.77}$$

for the 2D and axisymmetric geometries, respectively, where $t(x)$ is the slab thickness, w is the slab width, and $d(x)$ is the tube diameter (Fig. 2.15). The area divergence term is then

$$\text{2-D Slab:} \quad \frac{1}{A}\frac{\mathrm{d}A}{\mathrm{d}x} = \frac{t'(x)}{t(x)} \tag{2.78}$$

$$\text{Axisymmetric Tube:} \quad \frac{1}{A}\frac{\mathrm{d}A}{\mathrm{d}x} = 2\frac{d'(x)}{d(x)}, \tag{2.79}$$

where the prime ($\prime$) denotes differentiation with respect to the position x. As will be discussed below, the slope of the stream tube boundary in simple models is often given by a local matching of pressure and flow direction between the CJ (or von Neumann) state and the confinement and is assumed to remain constant through the reaction zone. If this is the case, then the slope will be the same in both 2D and axisymmetric geometries for a given shock or detonation velocity. If the magnitude of area divergence is small compared to the initial cross-sectional area of the stream tube (i.e., $t(0) >> L\, t'(x)$,

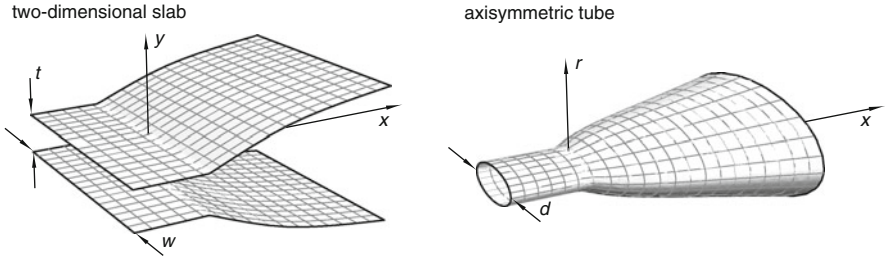

Fig. 2.15. Stream tubes in two-dimensional slab and axisymmetric, cylindrical geometries enclosing the reaction zone of a detonation wave. Note that the magnitude of area divergence and relative length of the reaction zone have been greatly exaggerated for this schematic

$d(0) >> L\, d'(x)$) where L is the length of the reaction zone, then the area divergence terms differ by a numerical factor of *two* for the two geometries

$$\text{2-D Slab:} \quad \frac{1}{A}\frac{\mathrm{d}A}{\mathrm{d}x} \approx \frac{t'(x)}{t(0)} \tag{2.80}$$

$$\text{Axisymmetric Tube:} \quad \frac{1}{A}\frac{\mathrm{d}A}{\mathrm{d}x} \approx 2\frac{d'(x)}{d(0)}. \tag{2.81}$$

This means that the solution for the reaction zone structure in the two geometries should be the same, provided the diameter of the axisymmetric cylinder is scaled by *twice* the thickness of the 2D slab.

Early models for detonation in finite-diameter charges by Jones [41] and Eyring et al. [27] used phenomenological descriptions for the stream tube area divergence (i.e., nozzle flow models). While not rigorous, these models are of interest in their providing a physical picture of the flow fields that result from the boundary of the charge expanding outward as the explosive reacts. The models developed by Jones and elaborated upon by Erying et al. assumed a Prandtl–Meyer (P–M) expansion fan originating where a normal detonation encountered the edge of the charge. The initial state was taken as the CJ state for the ideal, constant area detonation (note that using the subsonic von Neumann state is not an option since the P–M function is only defined for supersonic flow). For an unconfined charge, the P–M fan at the edge was matched to a stream tube containing the core of the detonation flow. For a heavily confined charge, the P–M fan was matched to an oblique shock transmitted into the confining material to determine the divergence angle, which was taken as constant. Eyring et al. went on to develop heuristic models incorporating the fact that, if the flow at the boundary of the charge is diverging outward following the leading shock, the shock front itself cannot be flat and must be oblique at the boundary. In other words, the leading shock front is curved (normal on the central axis of the charge and increasingly oblique toward the edges), similar to the meniscus of a liquid surface in a capillary tube. Eyring et al. were careful to point out that front curvature is a necessary consequence of diverging flow; curvature and flow divergence are different manifestations of the same phenomenon, not separate effects that should be superimposed in models. Theoretical investigations into the 1960s continued to presuppose functional forms for the stream tube area profile, often out of analytic convenience rather than from physical considerations [26, 100].

2.6.2 Radial Flow Derivative

Beginning with the work of Wood and Kirkwood [101], a more rigorous approach to solve for the reaction zone of a detonation wave with divergent flow was developed that examined the two-dimensional flow (either rectangular or axisymmetric) along the central axial streamline of the reaction zone.

Utilizing the fact that the flow is symmetric about this line, the continuity equation for two-dimensional, steady compressible flow

$$\nabla \cdot \left(\rho \overrightarrow{V}\right) = 0 \tag{2.82}$$

can be simplified for rectangular coordinates

$$\frac{\partial (\rho u)}{\partial x} + \frac{\partial (\rho v)}{\partial y} = 0 \tag{2.83}$$

since the transverse flow velocity v is zero along this streamline, as follows:

$$\frac{\partial (\rho u)}{\partial x} + \rho \frac{\partial v}{\partial y} = 0. \tag{2.84}$$

Note that, while the transverse velocity is zero along the central streamline ($v = 0$), the derivative of the velocity in the radial direction has a nonzero value $\left(\frac{\partial v}{\partial y} \neq 0\right)$. Likewise the continuity equation for axisymmetric flow in cylindrical coordinates

$$\frac{\partial (\rho u)}{\partial x} + \frac{1}{r}\frac{\partial (r\rho v)}{\partial r} = 0 \tag{2.85}$$

specialized to the central streamline via l'Hôpital's rule yields

$$\frac{\partial (\rho u)}{\partial x} + 2\rho \frac{\partial v}{\partial r} = 0. \tag{2.86}$$

The x-momentum equation in rectangular

$$\frac{\partial \left(\rho u^2\right)}{\partial x} + \frac{\partial (\rho u v)}{\partial y} = -\frac{\partial p}{\partial x} \tag{2.87}$$

and cylindrical coordinates

$$\frac{\partial \left(r\rho u^2\right)}{\partial x} + \frac{\partial (r\rho u v)}{\partial r} = -r\frac{\partial p}{\partial x} \tag{2.88}$$

both revert (via symmetry) to the familiar form of the momentum equation when applied along the axial streamline

$$\frac{\partial p}{\partial x} + \rho u \frac{\partial u}{\partial x} = 0. \tag{2.89}$$

Returning to continuity, (2.84) and (2.86) can be written as

$$\frac{\partial (\rho u)}{\partial x} + \alpha \rho \frac{\partial v}{\partial z} = 0, \tag{2.90}$$

where z denotes the transverse y-direction in the rectangular geometry and radial r-direction in the cylindrical geometry, and α has the value of 1 and

2 for the rectangular and cylindrical geometries, respectively. By comparing (2.90) with (2.4), the derivative of the transverse/radial velocity term ($\frac{\partial v}{\partial z}$) can be related to the area divergence of a stream tube

$$\frac{1}{A}\frac{\mathrm{d}A}{\mathrm{d}x} = \frac{\alpha}{u}\frac{\partial v}{\partial z}. \tag{2.91}$$

This equivalence can also be demonstrated by considering an arbitrarily small stream tube that encloses the flow along the charge axis, and using the derivative of the radial flow velocity to approximate the divergence of the stream tube boundary. As the stream tube shrinks to the axis, the correspondence (2.91) becomes exact.

2.6.3 Shock Front Curvature

The derivative of the radial flow velocity can also be related to the radius of curvature R of the leading shock front by using the geometric construction in the shock-attached reference frame shown in Fig. 2.16. The flow velocity approaching the shock is the detonation propagation velocity ($u_1 = D$). Note that this construction applies to the 2D slab and axisymmetric geometries equally. Using the fact that the component of flow velocity parallel $u_{\parallel} = D\sin\theta$ to a shock front does not change as the flow crosses the shock, as required by conservation of momentum, it is possible to express the radial component of velocity as

$$v = D\sin\theta\cos\theta - u_{\perp}\sin\theta. \tag{2.92}$$

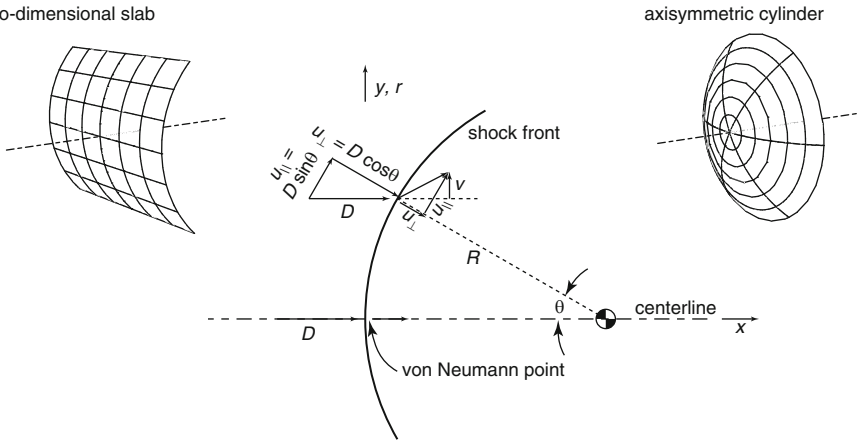

Fig. 2.16. Geometric construction relating shock front radius of curvature R to the derivative of the radial flow velocity $\frac{\partial v}{\partial r}$ or $\frac{\partial v}{\partial y}$ at the centerline immediately behind the shock

Performing a partial differentiation of the velocity v with respect to the angle θ

$$\left(\frac{\partial v}{\partial \theta}\right)_{\text{shock}} = D\left(\cos 2\theta\right) - u_{\perp}\cos\theta - \sin\theta\left(\frac{\partial u_{\perp}}{\partial \theta}\right)_{\text{shock}}, \tag{2.93}$$

where the "shock" subscript denotes that the differentiation was performed along the shock front. The differentiation can be converted to a differential with respect to y or r (denoted as z) as follows:

$$\left(\frac{\partial v}{\partial z}\right)_{\text{shock}} = \left(\frac{\partial v}{\partial \theta}\right)_{\text{shock}}\left(\frac{\partial \theta}{\partial z}\right)_{\text{shock}} = \frac{\left(\frac{\partial v}{\partial \theta}\right)_{\text{shock}}}{R\cos\theta}. \tag{2.94}$$

Taking the limit approaching the central axis

$$\lim_{\theta\to 0}\left(\frac{\partial v}{\partial z}\right) = \frac{D - u(0)}{R}, \tag{2.95}$$

where $u(0)$ is the axial velocity at the von Neumann point along the central axis. Thus, the radius of the curvature of the shock front is directly related to the derivative of the radial flow immediately behind the shock front. This relation applies strictly only at the von Neumann point (i.e., immediately after the leading shock); however, lacking further information, this derivative is often taken as constant through the reaction zone.

The shock radius R can be related to the curvature κ of the shock front as follows:

$$\kappa = \frac{\alpha}{R}, \tag{2.96}$$

where again α is 1 for the two-dimensional slab geometry (cylindrical curvature of the shock front) and 2 for the axisymmetric cylinder geometry (spherical curvature of the shock front). The fact that, for a locally steady detonation front, the shock curvature κ uniquely determines the eigenvalue velocity of propagation provides the means to construct the detonation front shape and trajectory as the detonation propagates, for example, through a complex charge geometry. This technique, called *Detonation Shock Dynamics*, is the subject of Chap. 7 of this volume.

2.6.4 Confinement Interaction via Newtonian Theory

In order to associate these divergent flow models with experimental results or make quantitative predictions of velocity deficits or critical diameter, it is necessary to link the flow divergence to the overall dimension (diameter or thickness) of the charge and the properties of the confinement. For condensed-phase detonations, solving for this interaction can be challenging; this topic is elaborated upon in Chap. 7 of the present volume. As an illustrative numerical example relevant to gaseous detonations, a simple Newtonian model for the interaction of the diverging flow in the reaction zone with the confinement will be developed further in this section. Being a nozzle flow-type model, it does not explicitly include the curvature of the shock front. However, this

model (originally proposed by Tsuge et al. [31, 95]) is instructive in that it treats the evolving interaction of the reacting flow with the confinement via an analytically tractable method without resorting to empirical input or an assumed formula for the area divergence.

The Newtonian model for hypersonic flow assumes that a flow encountering an inclined surface loses the component of velocity normal to the surface but retains the tangential velocity. In other words, a flow encountering an inclined surface slides along the surface, and the change in momentum flux of the flow determines that the pressure on the surface must vary as

$$p = p_\infty + \rho_\infty u_\infty^2 \sin^2 \beta, \tag{2.97}$$

where β is the surface inclination angle to the flow with freestream density ρ_∞, pressure p_∞, and velocity u_∞. Originally proposed by Newton, this flow model has been shown to be remarkably accurate in predicting surface pressures for slender bodies in hypersonic flow [4]. The model is invoked here to treat the flow of the confinement material as it encounters the expanding flow of reacting gas, thereby linking the pressure of the reacting flow to the divergence angle of the stream tube enclosing that flow. Since the stream tube cannot support a pressure difference, the reacting flow must locally match the pressure of the confinement and thereby the slope of the stream tube boundary. Using (2.97) for the flow of confinement material

$$p = p_c + \rho_c u_c^2 \sin^2 \beta = p_c + \rho_c u_c^2 \frac{\left(\frac{\mathrm{d}z}{\mathrm{d}x}\right)^2}{1 + \left(\frac{\mathrm{d}z}{\mathrm{d}x}\right)^2}, \tag{2.98}$$

where "c" denotes the properties of the confinement before interaction with the detonation wave and "z" is either the radius r or the half-thickness y of the stream tube. Solving for the slope of the stream tube

$$\frac{\mathrm{d}z}{\mathrm{d}x} = \sqrt{\frac{\frac{p(x)-p_c}{\rho_c u_c^2}}{1 - \frac{p(x)}{\rho_c u_c^2}}}. \tag{2.99}$$

This expression is used to find the area divergence term as a function of the local pressure in the stream tube

$$\text{2-D Slab:} \quad \frac{1}{A}\frac{\mathrm{d}A}{\mathrm{d}x} = \frac{t'}{t} = \frac{y'}{y} = \frac{1}{y}\sqrt{\frac{\frac{p(x)-p_c}{\rho_c u_c^2}}{1 - \frac{p(x)-p_c}{\rho_c u_c^2}}} \tag{2.100}$$

$$\text{Axisymmetric Tube:} \quad \frac{1}{A}\frac{\mathrm{d}A}{\mathrm{d}x} = 2\frac{d'}{d} = 2\frac{r'}{r} = \frac{2}{r}\sqrt{\frac{\frac{p(x)-p_c}{\rho_c u_c^2}}{1 - \frac{p(x)-p_c}{\rho_c u_c^2}}}. \tag{2.101}$$

These expressions for $\frac{1}{A}\frac{\mathrm{d}A}{\mathrm{d}x}$ can be used directly in the ODE governing the reaction zone structure (2.75). Since pressure now appears explicitly, this ODE must be integrated coupled to the momentum equation (2.5) reproduced here

$$\frac{\mathrm{d}p}{\mathrm{d}x} = -\rho u \frac{\mathrm{d}u}{\mathrm{d}x} = -\frac{\dot{m}}{A}\frac{\mathrm{d}u}{\mathrm{d}x} \tag{2.102}$$

which can be related to the local streamtube dimension as follows:

$$\text{2-D Slab:} \quad \frac{\mathrm{d}p}{\mathrm{d}x} = -\rho_1 u_1 \frac{y_1}{y}\frac{\mathrm{d}u}{\mathrm{d}x} \tag{2.103}$$

$$\text{Axisymmetric Tube:} \quad \frac{\mathrm{d}p}{\mathrm{d}x} = -\rho_1 u_1 \left(\frac{r_1}{r}\right)^2 \frac{\mathrm{d}u}{\mathrm{d}x}, \tag{2.104}$$

where ρ_1 and u_1 are the density and velocity upstream of the detonation ($u_1 = D$) and y_1 and r_1 are the initial half-thickness and radius of the explosive, respectively.

This set of ODE's was integrated to obtain the structure of a detonation with yielding confinement. The properties of the explosive were the same that have been used previously in this chapter ($\gamma = 1.2$, $Q = 10$, and a single-step Arrhenius reaction with $\frac{E_a}{RT_1} = 25$). The inert confinement was assumed to be at the same initial pressure as the explosive, but with a density 2.5 times greater than the explosive ($\rho_c = 2.5\rho_1$). This density ratio approximately corresponds to the density ratio of air to stoichiometric hydrogen/oxygen, which will be used as an illustrative experiment later in this section. As expected from the form of the governing ODE (2.75), where the effect of area divergence from the yielding confinement is seen to compete with exothermic heat release, it is necessary to iterate upon the detonation velocity to find an eigenvalue solution that can pass smoothly through the sonic point without encountering a singularity. As was seen previously with the effect of heat transfer and friction, there is a critical amount of loss that the detonation can sustain, in this case, resulting from the explosive charge being too thin and losing too much momentum to the divergence of the flow. For charges thinner than this critical thickness, no steady solution with a sonic point can be found.

The structure of the reaction zone for the critical slab thickness at which failure occurs (i.e., at the critical turning point) is shown in Fig. 2.17 as thick lines in comparison to the ideal CJ solution for an infinite thickness charge (thin lines). A small schematic done to scale is included to show the actual amount of area divergence observed at the critical turning point. All dimensions are normalized by the half reaction thickness of the ideal CJ detonation ($L_{1/2}$). The location of reaction completion or the sonic surface cannot be defined for the ideal CJ detonation. The sonic surface for the finite-size charge with area divergence, however, can be determined from the eigenvalue solution. Note that the area divergence from the shock to the sonic plane is moderate (≈30% increase in area) and that, even for the smallest charge thickness that can support detonation, the thickness of the explosive slab is still more than three times the length of the detonation front (i.e., the distance from the shock to the sonic surface). In comparison to the ideal CJ solution, the location of the peak in exothermicity and half reaction length have more than quadrupled due to the lower post-shock temperature, and the exothermicity is still finite as the solution passes through sonic. At the sonic surface

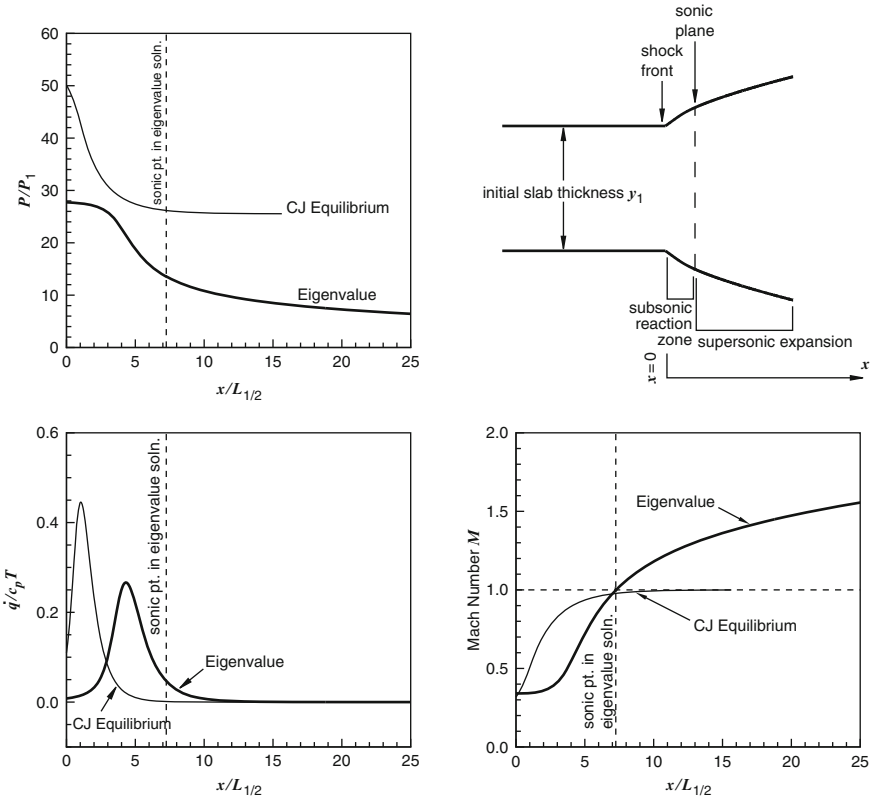

Fig. 2.17. Structure of detonation in a two-dimensional slab at the critical turning point (critical slab thickness), showing pressure, heat release rate, and flow Mach number ($\frac{E_a}{RT_1} = 25$, $Q = 10$, $\gamma = 1.2$, and confinement $\rho_c = 2.5\rho_1$). The ideal CJ solution (without flow divergence) is also shown as a *thin line* for each variable. A silhouette of the quasi-1D stream tube is also shown to scale

approximately 96% of the available chemical energy has been released. This effect in isolation would only result in an approximately 2% velocity deficit. Thus, the observed velocity deficit (about 25% below CJ) is predominately due to a loss in directed axial momentum from the area divergence and is not due to the sonic surface isolating chemical energy release from the shock front.

The eigenvalue velocity is plotted (normalized by the ideal CJ velocity) as a function of the charge diameter or thickness in Fig. 2.18. Following the convention of the condensed-phase explosives literature, the detonation velocity is plotted as a function of the inverse thickness ($\frac{1}{2t}$) or inverse diameter ($\frac{1}{d}$). The inverse of the dimension is used so that extrapolation of the velocity to the y-axis intercept should yield the ideal (infinite diameter) CJ velocity. The factor of two is used in plotting the results as a function of thickness due

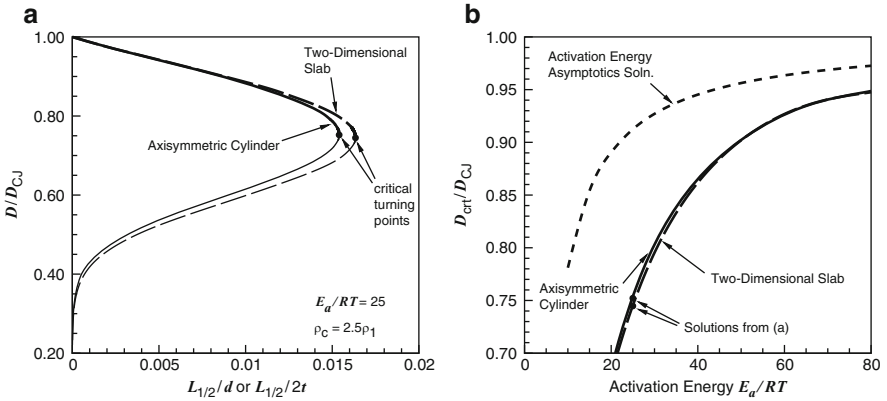

Fig. 2.18. (**a**) Detonation velocity as a function of the charge diameter (axisymmetric cylindrical charge) or thickness (two-dimensional slab charge), with the stable branch shown as a *heavy line*, the nonphysical branch as a *thin line*, and the critical turning points denoted as *dots*. (**b**) Detonation velocity at the critical turning point as a function of activation energy. The activation energy asymptotic analysis of [38, 45, 105] is also shown

to the approximate 2:1 scaling expected between the slab and axisymmetric geometries, as discussed in Sect. 2.6.1. For a sufficiently large initial thickness or diameter, two detonation solutions are found, similar to detonations with heat transfer and friction losses discussed in Sect. 2.4. Again, the lower branch, which exhibits a nonphysical increase in detonation velocity with decreasing thickness, is ruled out as unstable. As the thickness or diameter is decreased, the velocity of the upper (physical) branch decreases until a critical turning point is encountered; any further decrease in the explosive charge dimension is expected to result in detonation failure. The approximate 2:1 scaling expected between results with a 2D slab charge and an axisymmetric cylindrical charge is confirmed.

As activation energy increases, the magnitude of velocity deficit that the detonation can tolerate before failure decreases, as well as the relative amount of area divergence and the effective "thickening" of the wave that can be sustained. The effect of activation energy on the critical thickness and diameter of two-dimensional slabs and axisymmetric tubes was studied systematically using the Newtonian model for diverging flow interaction with confinement in Fig. 2.18b. For values of activation energy representative of real detonable mixtures ($\frac{E_a}{RT_1} = 30 - 80$), the critical velocity occurs at 80–95% of the ideal CJ detonation velocity.

Similar to the solution for detonations with heat loss by Zeldovich and Kompaneets discussed in Sect. 2.4.4, it is possible to perform an asymptotic analysis of the reaction zone structure in the limit of very high activation energy. Such analysis has been done by He and Clavin [38], Yao and

Stewart [105], and Klein et al. [45]. The analysis by [38] and [45] yields a result for the critical velocity identical to that previously found by Zeldovich and Kompaneets for detonations with heat loss (2.38), reproduced here

$$\frac{D_{\mathrm{crt}}}{D_{\mathrm{CJ}}} \approx 1 - \frac{1}{2}\frac{1}{\left(\frac{E_a}{RT_{\mathrm{vN}}}\right)}. \tag{2.105}$$

The analysis of [105] produces a slightly more complex expression dependent upon γ, which nonetheless is equivalent to (2.105). This relation is plotted in Fig. 2.18 as a dashed line. While exhibiting qualitatively similar trends to the results obtained by integrating the governing ODEs to find the eigenvalue detonation velocity, quantitative agreement is only found for very high values of activation energy (where the asymptotic analysis is intended to apply).

2.6.5 Comparisons to Experiment

Experiments with columns of detonable gas (hydrogen/oxygen) confined by inert gas (nitrogen) have been performed by [18, 83, 84, 97]. Some characteristic images of successful propagation and failure of propagation are shown in Fig. 2.19; further experiments are discussed in Chap. 4 of this volume. The expansion of the detonation products and the oblique shock being driven into the confining gas are clearly visible, as is the curvature of the shock front. Quantitative comparison of the measured detonation velocity in these finite-diameter columns of detonable gas with ZND-type calculation using the Newtonian model for interaction with the confinement (as was done in Sect. 2.6.4, but with a more detailed chemistry model) was done by Tsuge et al. [31, 95] and showed general agreement with the experiments. The experimental data, however, had relatively large error bars, and more accurate velocity measurements would necessitate measuring propagation in longer columns of detonable gas, which is a difficult experiment to prepare.

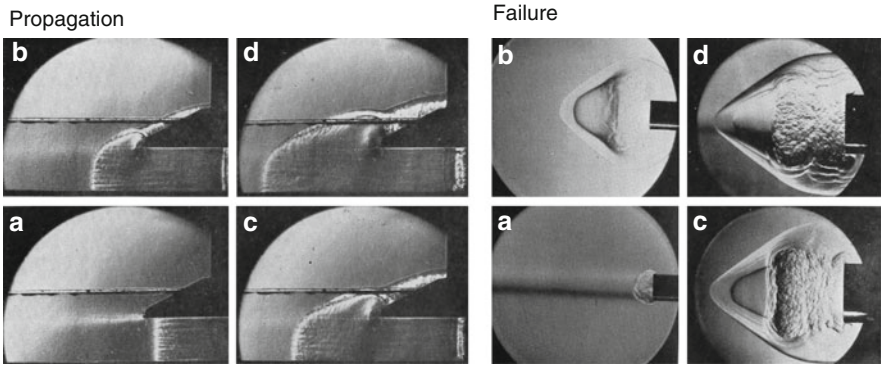

Fig. 2.19. Experimental photographs of detonations in finite-diameter, unconfined columns of hydrogen/oxygen [83]

Perhaps the most impressive demonstration linking the ZND model to an experimental result is the study of gaseous detonations in porous-walled tubes and channels of Radulescu [68, 70]. Due to the flow into the porous walls, the reaction zone of the detonation in such a tube or channel experiences a divergent flow, qualitatively similar to the divergence resulting from yielding confinement or boundary layers discussed earlier in this section. This divergence results in velocity deficits and, for a sufficiently small tube diameter, failure of the detonation. The experimental measurements of the velocity deficit and failure diameter in mixtures of hydrogen/oxygen and acetylene/oxygen with large amounts of argon dilution exhibited good correlation with a ZND calculation with detailed chemistry (similar to that in Sect. 2.5) which includes the effect of flow divergence (as is done in this section). The radial flow derivative (or, equivalently, the area divergence) was estimated by assuming that the flow into the porous wall was choked (sonic) at the pore openings, with the net outflow being scaled by the porosity of the wall. Comparisons of this model demonstrated good agreement with the experimental results, including prediction of the critical diameter at which detonation failure was observed (see Fig. 2.20). What is more, studies in porous-walled tubes and porous-lined

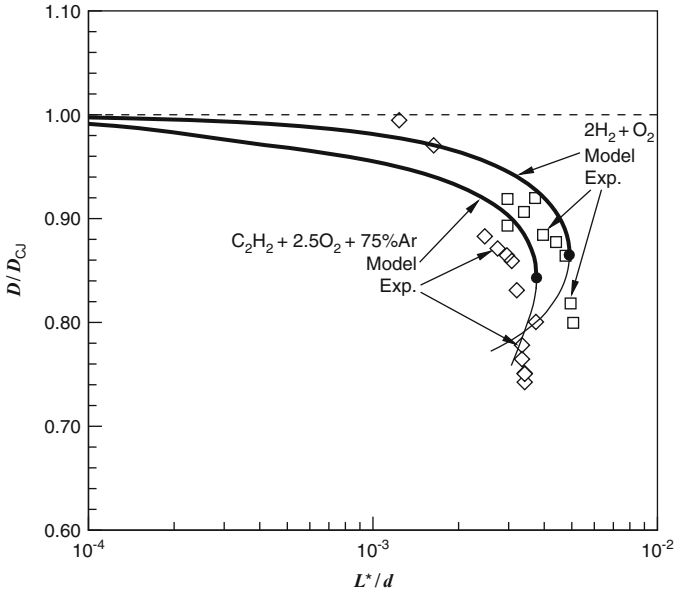

Fig. 2.20. Velocity deficits observed for gaseous detonations propagating in porous-walled tubes, compared to a ZND model with area divergence due to flow into the tube walls. The tube diameter d is normalized by the computed reaction zone length of the ZND detonation with divergence, L^*. In the experiments, initial pressure was changed in order to vary reaction zone length while the tube diameter was constant [68]

channels (with porous surfaces only on the upper and lower wall, with the side walls being impermeable) recovered the 2:1 scaling between the two geometries, as predicted by weak area divergence and front curvature theory. Interestingly, however, this excellent agreement was only obtained in hydrogen/oxygen mixtures and acetylene/oxygen mixtures with large amounts of argon dilution. While these mixtures exhibit the cellular structure characteristic of all gaseous detonations, the cellular structure in these particular mixtures is remarkably regular and is believed to be a piecewise laminar ZND-type structure, with the transverse waves not contributing significantly to the burning mechanism within the front. When these experiments were repeated in acetylene/oxygen mixtures with little or no argon dilution, which exhibit an irregular cellular structure, the agreement with the ZND calculations and the 2:1 scaling between geometries no longer occurred (i.e., the detonation continued to propagate in smaller diameter tubes and with larger velocity deficits for which the ZND calculation would predict failure, and the scaling between diameter and channel height became 1:1 in these cases). These results strongly suggests that detonation propagation in mixtures with irregular cellular structure, which are known to exhibit significant amounts of burning in the transverse waves of the cells, is controlled by the cellular structure of the wave and can no longer be described by a laminar, ZND-type model.

2.7 Concluding Remarks

The appeal of the ZND model lies in its ability to be easily implemented via numerical integration of ordinary differential equations with high confidence in the results (e.g., nearly all of the figures in this chapter were generated with a relatively few lines of code in *Mathematica* utilizing the built-in ODE solver NDSolve). The limitations of the ZND model come from its assumptions of an essentially laminar, one-dimensional structure and steadiness. As the remainder of this book exemplifies, the real dynamics of detonation waves is dominated by multidimensional and transient effects. Ultimately, even multidimensional, transient simulations of detonations must be averaged back onto a one-dimensional representation in order to be digested, such as in the recent study by Radulescu et al. [71].

Besides the presence of multidimensional structure and transient dynamics, other "breakdowns" of the ZND model can occur if the reaction zone is no longer spatially resolved from the shock front. The scenario of reactions occurring within the shock front itself due to "ultrafast" chemistry was explored via Direct Simulation Monte Carlo calculations by Anderson and Long [2,3]. The detonation structures observed were identified as weak detonations that proceeded from the initial state along the Rayleigh line directly to the product Hugoniot. While detonations of this type are improbable in real gases, since such very reactive mixtures are unlikely to be sufficiently metastable to be explored experimentally, similar phenomena might exist in polycrystalline

condensed-phase explosives due to the dispersed nature of the shock and localized reactions at hot spots. Evidence of the lack of a von Neumann spike has been reported in experiments in which laser light, reflected off the interface between high explosives (e.g., RDX, HMX, etc.) and a water window, was used to measure the particle velocity as the detonation emerged. The laser interferometry measurements showed a monotonically increasing velocity (corresponding to a monotonically increasing pressure) through the shock/reaction complex as the detonation crossed the interface [47,96], although these results remain controversial. Outside of these exceptions, the ZND framework remains the foundation upon which transient and multidimensional treatments of detonations are built.

A principal theme of this chapter has been that any energetic material is capable of exhibiting detonation wave propagation and that only in the presence of losses at the boundaries can limits to detonation propagation be meaningfully defined (Khariton's principle). This proposition has motivated the consideration of detonations in media that are so extremely dilute that they would not seem detonable. The interstellar medium is one such example [94]. Some models for waves of star formation treat them as detonation waves, wherein the energy released by supernovae or newly ignited stars drives shock waves into the interstellar media, compressing the media and promoting further nucleation of stars (i.e., self-propagating star formation). The spiral arms of galaxies such as our own Milky Way have been speculated to be just such waves [16, 29, 33, 81]. Other possible astrophysical appearances of detonation waves are reviewed by Oran [61].

Another reoccurring theme in this chapter is that factors competing with the effect of exothermic energy release to accelerate the flow in the reaction zone (e.g., friction, endothermic chemical reaction, area divergence, etc., all of which act to decelerate the flow) result in the flow passing through a sonic point (saddle condition) at a nonequilibrium state, qualitatively similar to the converging/diverging nozzle of compressible flow. The solution for the reaction zone in this case is an eigenvalue of the governing differential equations, in contrast to the classical equilibrium CJ theory. It is interesting to note that essentially the same dynamics occur in other natural phenomena and technological applications. The acceleration of the initially subsonic solar wind leaving the sun's surface to supersonic flow into interstellar space without passing through a physical throat (i.e., the flow is entirely divergent) was hypothesized in a seminal study by Parker [64] to result from a saddle point condition where the divergence of the flow balances a body force term resulting from the sun's gravity. An application more closely related to detonation flow fields is the dual-mode ramjet/scramjet [17]. In this aerospace propulsion concept, a single engine geometry is able to realize both subsonic and supersonic combustion regimes, depending on the flight Mach number of the vehicle. In ramjet mode, the engine would exploit the combined effect of exothermic reaction and area divergence to continuously accelerate the flow from subsonic to supersonic without having to pass through a local minimum in area (i.e., a

nozzle throat). Similar "transonic" combustion regimes are believed to occur in ram accelerators [39,73]. A dynamical systems analysis of the critical points in these type of flows was recently performed by De Sterck [86].

Researchers who have labored to develop the framework for understanding detonation waves should derive satisfaction that their efforts may find a wider range of application than the narrow field for which that framework was originally developed.

Acknowledgments

This chapter was developed out of discussions with Jimmy Verreault, Oren Petel, François-Xavier Jetté, Patrick Batchelor, and David Mack. Vincent Tanguay contributed to the analysis of the inclusion of the work done by friction in detonations and the Taylor wave analysis in the appendix. Jean-Philippe Dionne's doctoral dissertation provided a template for much of this chapter. Jenny Chao and Matei Radulescu are thanked for sharing their experimental data. Fan Zhang and Craig Tarver provided helpful and insightful commentary.

A.1 Appendix A: Gasdynamics of Detonation Products

The existence of sonic flow at the exit plane of a detonation, which comprises the classical Chapman–Jouguet condition and its generalization to nonideal detonations, means that the detonation wave is decoupled from the expansion of the detonation products in the wake of the wave. Thus, the details of the expansion do not need to be explicitly considered in solving for the detonation wave properties or structure. The expansion of the gas that has been processed by the detonation (i.e., the burned gas) can be of interest in its own right for some applications. Consideration of how the detonation exit state is matched with the downstream expansion can also provide some guidance in determining the possible non-CJ exit states that might be realizable. The gasdynamics of the unsteady expansion of detonation products was treated by G.I. Taylor in a seminal work [93], and the solution he found is often referred to as the *Taylor wave*. In this appendix, the Taylor wave flow field solution is briefly developed using the method of characteristics for the planar case (Sect. A.1.1), matching of the Taylor wave with different branches of detonation solutions is then examined (Sect. A.1.2), and finally a more formal similarity solution for the cylindrical and spherical case (Sect. A.1.3) is developed.

A.1.1 Planar Detonation

Taylor's treatment of the dynamics of the products emerging from a planar detonation begins by assuming that the detonation wave propagates at a

steady speed, with the products leaving the wave at constant conditions. It is further assumed that there are no shock waves in the flow downstream of the detonation. Thus, since all the flow originates at the same state (denoted state "2" to be consistent with the notation in this chapter) and remains isentropic, the entire flow has the same value of entropy (i.e., the flow is homentropic). This means that, at every point in the flow, $u' - c$ characteristic waves originating from the detonation but propagating in the opposite direction as the wave have the same value of the Riemann invariant:

$$C_- = u' - \frac{2}{\gamma - 1}c = u'_2 - \frac{2}{\gamma - 1}c_2, \tag{2.106}$$

where the prime ($'$) on u' is used to denote that it is the velocity in the unsteady, laboratory-fixed reference frame, in order to differentiate it from the steady flow velocity used throughout this chapter. From (2.106), it can be shown that at every point in the products, u' and c are linearly related. This result means that $u' + c$ characteristics (along which $C_+ = u' + \frac{2}{\gamma-1}c =$ constant) that propagate in the detonation products toward the wave must have constant values of u' and c and are therefore straight lines in the (x, t) plane.

One possible solution that can be constructed with straight $u' + c$ characteristics is a centered rarefaction fan originating at the origin. The detonation is also assumed to originate at the origin and has negligible thickness compared to the domain of interest. Thus, the flow pattern becomes self-similar, as seen in Fig. 2.21. At any point inside the centered rarefaction, the value

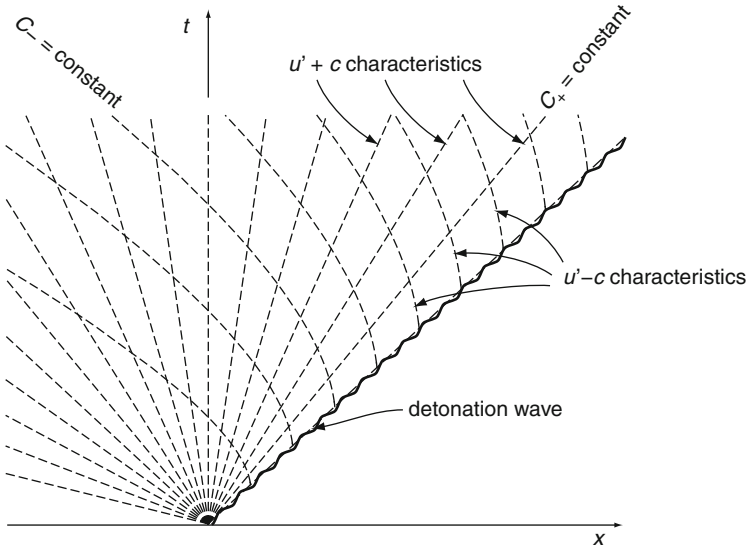

Fig. 2.21. Centered rarefaction solution for the expansion of products behind a detonation wave, showing the $u' + c$ and $u' - c$ characteristics

of $u' + c$ must equal the value of $\frac{x}{t}$ at that point. Using this property, along with the constant C_- characteristics emanating from the detonation, the flow velocity and sound speed can be solved for:

$$u'(x,t) = \frac{2}{\gamma+1}\left(\frac{x}{t} - c_2\right) + \frac{\gamma-1}{\gamma+1}u_2' \tag{2.107}$$

$$c(x,t) = \frac{\gamma-1}{\gamma+1}\left(\frac{x}{t} - u_2'\right) + \frac{2}{\gamma+1}c_2. \tag{2.108}$$

Note that position and time always appear as the combination $\frac{x}{t}$, verifying that this is a similarity solution. The other thermodynamic properties (pressure, density, temperature) can be determined from the sound speed by using the isentropic relations. The velocity profile behind the wave is plotted in Fig. 2.22. For this particular plot, the conditions at the detonation exit plane were taken as the CJ conditions in the limit of large heat release

$$\lim_{Q\to\infty}\frac{u_2'}{D} = \frac{1}{\gamma+1}, \quad \lim_{Q\to\infty}\frac{c_2}{D} = \frac{\gamma}{\gamma+1},$$
$$\lim_{Q\to\infty}\frac{\rho_2}{\rho_1} = \frac{\gamma+1}{\gamma}, \quad \lim_{Q\to\infty}\frac{p_2}{\rho_1 D^2} = \frac{1}{\gamma+1}, \tag{2.109}$$

where a value of $\gamma = 1.2$ was used for Fig. 2.22. Note that the velocity in the centered rarefaction fan goes to zero and reverses direction, reaching an escape speed of

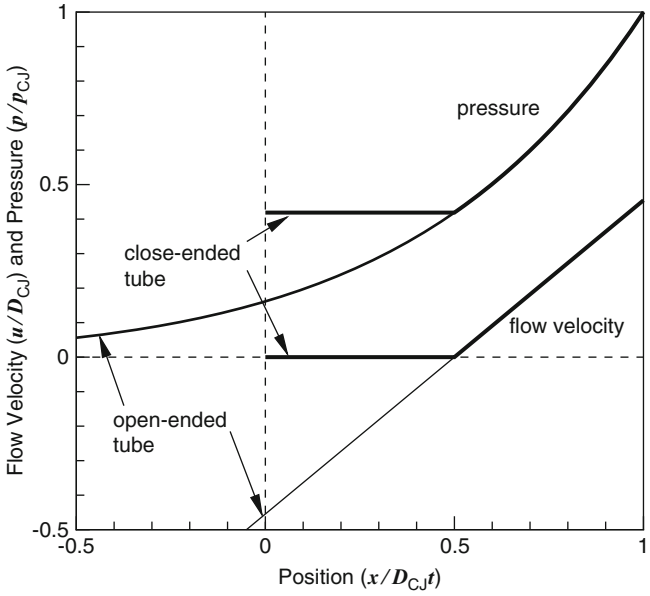

Fig. 2.22. Flow field behind a planar CJ detonation wave (Taylor wave) showing pressure and flow velocity for both close-ended and open-ended tubes ($\gamma = 1.2$)

$$\lim_{c\to 0} \frac{u}{D} = -\frac{1}{\gamma - 1} \tag{2.110}$$

as the flow expands to zero pressure and temperature, with the flow being directed in the $-x$ direction. This solution would correspond to the case where detonation is initiated in a tube with an evacuated semi-infinite region ($x < 0$). For the more familiar case of a detonation initiated at the closed end of a tube, the rarefaction fan can be truncated once the product flow has been brought to rest ($u' = 0$) and then remains uniform from this point to the endwall. The trailing edge of the rarefaction in this case propagates at $c_3 = c_2 - \frac{\gamma-1}{2}u_2'$. The fraction of the tube containing gas at rest can be shown to be

$$\frac{c_3}{D} = 1 - \frac{\gamma + 1}{2}\frac{u_2'}{D}. \tag{2.111}$$

In the limit of a high heat release detonation, this fraction is exactly $\frac{1}{2}$, meaning half the gas behind the detonation is a rest.

When applying the Taylor wave solution to gas-phase detonations propagating in a tube, the flow may be significantly modified by heat transfer and friction to the tube walls, and the solution is no longer self-similar. This problem was treated by [25, 79, 80]; for a more modern treatment, see Radulescu and Hanson [69].

A.1.2 Matching Expansion to Detonation Exit State

How the unsteady expansion downstream of the wave can be matched with the steady detonation front is now examined. In the previous section, it was assumed that the detonation was a CJ detonation, meaning that the products exit the wave at $u_2' = D_{\mathrm{CJ}} - c_2$. In this case, the leading edge of the centered rarefaction (i.e., the Taylor wave) will have a speed $u_2' + c_2 = D_{\mathrm{CJ}}$ and thus will remain parallel to the detonation in the (x, t) plane, as shown in Fig. 2.23a. Thus, the sonic surface permits the steady detonation to match the unsteady rarefaction in the products downstream of the detonation.

If a weak detonation with supersonic exit flow is considered ($u_2 > c_2$), then $u_2' + c_2 < D$ and thus centered rarefactions can never reach the detonation. In this case, an ever increasing, uniform column of gas at the weak detonation exit state will form between the head of the rarefaction and the detonation front. This scenario is illustrated in Fig. 2.23b.

Finally, if a strong detonation is considered, then $u_2 < c_2$ (subsonic exit flow), so that $u_2' + c_2 > D$, and any $u' + c$ wave will overtake the detonation. In this case, it is not possible to construct a similarity solution with a centered rarefaction. Other solutions can be found to exist for a strong detonation, with a piston-supported detonation being one example, where straight $u + c$ characteristics emanating from the piston face continuously merge with the detonation as shown in Fig. 2.23c. If the piston were suddenly stopped, then the rarefactions generated would begin to interact with the detonation, resulting in its deceleration until a limiting characteristic became parallel with the

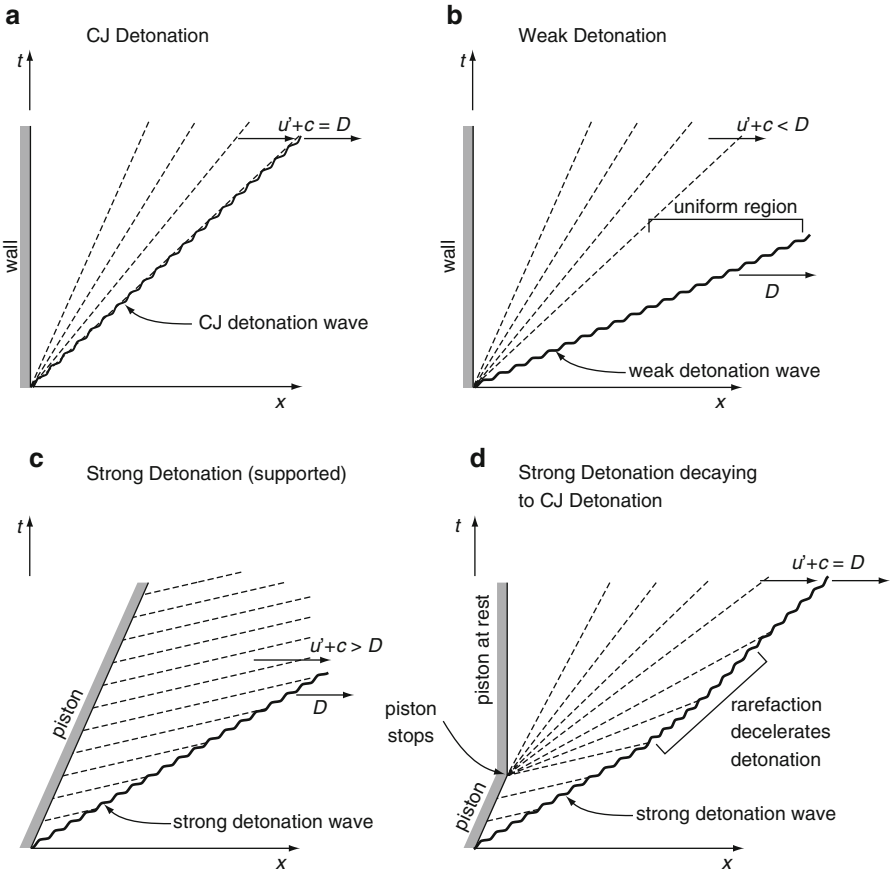

Fig. 2.23. Expansion of combustion products behind a detonation wave for the cases of (**a**) CJ detonation, (**b**) weak detonation, (**c**) strong (piston-supported) detonation, and (**d**) a piston-supported detonation in which the piston stops and the rarefactions generated overtake detonation, decelerating it until the detonation is parallel with $u' + c$ characteristics (CJ detonation)

detonation, establishing a CJ detonation. This simple picture, illustrated in Fig. 2.23d, perhaps provides a more satisfying explanation for the legitimacy of the CJ condition of sonic flow at the exit of an unsupported detonation wave.

A.1.3 Cylindrical and Spherical Detonations

To construct a solution for the dynamics of the products behind a spherical detonation originating from a point (or a cylindrical detonation initiated along a line), the conservation of mass and momentum for spherical and cylindrical symmetry are used as follows:

$$\frac{\partial \rho}{\partial t} + \rho \frac{\partial u}{\partial r} + u \frac{\partial \rho}{\partial r} + \alpha \frac{\rho u}{r} = 0 \tag{2.112}$$

$$\frac{\partial u}{\partial t} + u \frac{\partial u}{\partial r} + \frac{1}{\rho} \frac{\partial p}{\partial r} = 0, \tag{2.113}$$

where $\alpha = 1, 2$ for cylindrical and spherical geometries, respectively (note that for $\alpha = 0$ the equations revert to planar), and u is the velocity in the laboratory-fixed frame. Following the notation of [89], the following nondimensional variables are introduced:

$$\xi = \frac{r}{Dt}, \quad \psi = \frac{\rho}{\rho_2}, \quad \phi = \frac{u}{D}, \quad f = \frac{p}{\rho_2 D^2}. \tag{2.114}$$

Taking ξ as the independent variable of a similarity solution, the governing PDE's become ODE's and the differentials can be solved for

$$\begin{aligned} \phi'(\xi) &= \frac{f'}{\psi(\xi - \phi)} \\ \psi'(\xi) &= \frac{\alpha \psi \phi (\xi - \phi) + \xi f'}{\xi (\xi - \phi)^2}. \end{aligned} \tag{2.115}$$

In order to evaluate f', an equation of state of the form $f(\psi)$ is required. Here, the ideal gas equation for an isentropic process will be used ($\frac{p}{\rho^\gamma} =$ constant); implementation of equations of state more relevant to condensed-phase explosives is considered by [89]. For an ideal gas,

$$f'(\psi) = \left(\frac{\gamma}{\gamma + 1} \right)^2 \psi^{\gamma - 1} \psi'. \tag{2.116}$$

When this expression is used in (2.115) along with (2.109), the differential equations become singular at the exit plane of the CJ detonation (i.e., the denominators of both equations go to zero as $\xi \to 1$). Thus, while flow properties are constant at the exit plane of the detonation, their spatial derivatives would be infinite in the case of a CJ detonation. In order to circumvent this issue, Taylor [93] constructed a local, approximate solution in the vicinity of the detonation front, and then began a numerical integration an arbitrarily small distance from the front (e.g., at $\xi = 0.999$) and integrated inward. Alternatively, it is possible to just arbitrarily assume values slightly perturbed from their CJ values in order to initiate the numerical integration and still obtain reasonable results.

Such a numerical integration of (2.115) was performed for a spherical wave ($\alpha = 2$) and the results shown in Fig. 2.24, where the velocity ratio $\frac{u}{D} = \phi$ and pressure ratio ($\frac{p}{p_{\mathrm{CJ}}} = \psi^\gamma$) are plotted for a value of γ representative of a gas-phase detonation ($\gamma = 1.2$). Also shown is the structure of the Taylor wave for a value of $\gamma = 3$. This value of γ is often used as a crude approximation for the products of condensed-phase explosives, and fitting of γ to more sophisticated equations of state usually results in values in this vicinity [89]. From Fig. 2.24,

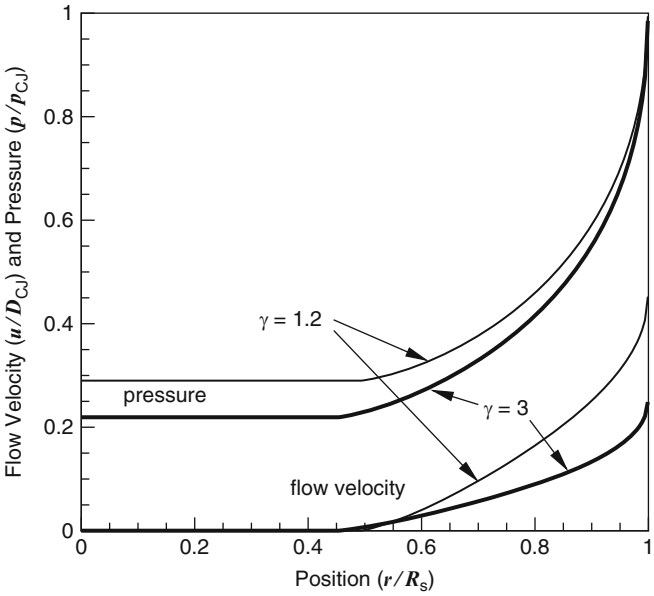

Fig. 2.24. Flow field behind a spherically expanding CJ detonation wave (Taylor wave) showing pressure and flow velocity for the cases of a gas-phase detonation ($\gamma = 1.2$) and condensed-phase detonation ($\gamma = 3$)

it can be seen that the flow reaches zero velocity at approximately halfway between the detonation front and the origin. The solution is truncated at that point, and constant conditions are assumed from there to the center in order to avoid the solution for density and flow velocity asymptoting to nonphysical, negative infinity as the solution approaches the center (note that constant values of density and velocity are also valid solutions of (2.115), so the solution can be truncated at any point and replaced with constant values). The pressure at the center of the spherical wave is approximately one-third to one-fifth of the CJ detonation pressure.

Note that if $\alpha = 0$ is used in (2.115) for the planar geometry, the numerators are zero and either trivial behavior is obtained (i.e., the differentials of flow velocity and density are zero and thus the flow is uniform behind the front) or the denominators must also be zero. Imposing the latter condition can be shown to be equivalent to the planar solution constructed via the Method of Characteristics in Sect. A.1.1.

The fact that the solutions for detonation products in the cylindrical and spherical cases become singular at the detonation front when the CJ conditions are imposed was a source of concern for some early researchers, leading some of them to even suggest that spherically expanding detonations might not exist [15, 42]. Spherical detonations were experimentally obtained as early as 1925 [49], but the issue was still debated into the 1960s. Lee et al. pointed

out that initiation of a spherical detonation will always likely require some degree of initial overdrive that will result in the detonation being initially on the strong branch of the solution ($u' + c > D$) and will only asymptotically approach an ideal CJ detonation as the wave expands, so that the issue of the infinite gradients in the solution is avoided [50].

A.2 Appendix B: Critical Sonic Point with Friction

For a detonation with friction (and no heat transfer), the critical condition at which the wave propagation velocity equals the velocity of the combustion products can be solved for analytically as follows [7, 20]. The momentum and energy equations (2.27) and (2.28) can be equated (excluding the heat loss term) via the friction factor

$$\mathrm{d}\left(p + \rho u^2\right) = \mathrm{d}\left[\rho \frac{u}{u_1}\left(h + \frac{1}{2}u^2\right)\right] = f\mathrm{d}x \tag{2.117}$$

and integrated to yield

$$p + \rho\left(u^2 - \frac{u}{u_1}\left(h + \frac{1}{2}u^2\right)\right) = C_1, \tag{2.118}$$

where C_1 is a constant of integration that can be evaluated using conditions upstream of the detonation wave (u_1, p_1, ρ_1, and $h_1 = c_p T_1$). At the critical sonic condition, the flow exiting the wave is sonic and equal to the velocity of the flow approaching the wave (in the laboratory-fixed frame, this is equivalent to the flow that has been processed by the wave being at rest),

$$u_{2_{\mathrm{crs}}} = c_{2_{\mathrm{crs}}} = D_{\mathrm{crs}}, \tag{2.119}$$

where the "2" subscript designates the exit state. The condition that exit velocity is the same as the inflow velocity means that the density is constant across the wave ($\rho_1 = \rho_2$). These relations allow the critical Mach number of propagation to be solved for

$$M_{\mathrm{crs}} = \frac{D_{1_{\mathrm{crs}}}}{c_1} = \sqrt{\gamma Q + 1}. \tag{2.120}$$

Since the density is constant across the wave, this critical sonic condition corresponds to a front of constant volume explosion propagating through the medium with a pressure increase given by

$$\frac{p_{2_{\mathrm{crs}}}}{p_1} = \frac{p_{\mathrm{CV}}}{p_1} = \gamma Q + 1. \tag{2.121}$$

At this critical sonic condition, the flow velocity being zero relative to the wall at the exit of the wave means that friction no longer influences the flow

at that point, and thus it is no longer possible to find an eigenvalue solution that passes through a sonic point. At lower wave velocities, the flow will be entirely subsonic from the shock to the rear boundary condition (i.e., no sonic condition can be found). To continue the solution curve in Fig. 2.7 to lower velocities, a different criterion is adopted, namely that the flow velocity must be zero in the laboratory-fixed frame, satisfying a closed end-wall boundary condition. This solution may have some relevance to the so-called "choking regime" of combustion wave propagation that is experimentally observed in combustible mixtures in obstacle laden tubes, as discussed in Sect. 2.4.5.

References

1. Akyurtlu, A.: An investigation of the structure and detonability limits of hydrogen-chlorine detonations, PhD Thesis, University of Wisconsin-Madison (1975)
2. Anderson, J.B., Long, L.N.: Direct Monte Carlo simulation of chemical reaction systems: Prediction of ultrafast detonations. J. Chem. Phys. **118**(7), 3102–3110 (2003)
3. Anderson, J.B., Long, L.N.: Direct simulation of pathological detonations. In: Ketsdever, A.D., Muntz, E.P. (eds.) Rarefied Gas Dynamics. American Institute of Physics Conference Series, vol. 663, pp. 186–193 (2003)
4. Anderson J. Jr.: Hypersonic and High-Temperature Gas Dynamics, AIAA Education Series, 2nd edn., 813pp. AIAA, Restons (2006)
5. Bauer, P.A., Dabora, E.K., Manson, N.: Chronology of early research on detonation wave. In: Kuhl, A.L., Leyer, J.C., Borisov, A.A., Sirignano, W.A. (eds.) Dynamics of Detonations and Explosions: Detonations. Progress in Astronautics and Aeronautics, vol. 133, pp. 3–18. AIAA, VA (1991)
6. Brailovsky, I., Sivashinsky G.: On deflagration-to-detonation transition. Combust. Sci. Technol. **130**(1), 201–231 (1997)
7. Brailovsky, I., Sivashinsky, G.: Hydraulic resistance and multiplicity of detonation regimes. Combust. Flame **122**(1–2), 130–138 (2000)
8. Brailovsky, I., Sivashinsky, G.I.: Hydraulic resistance as a mechanism for deflagration-to-detonation transition. Combust. Flame **122**(4), 492–499 (2000)
9. Brailovsky, I., Sivashinsky, G.: Effects of momentum and heat losses on the multiplicity of detonation regimes. Combust. Flame **128**(1–2), 191–196 (2002)
10. Brinkley S.R. Jr., Richardson J.M.: On the structure of plane detonation waves with finite reaction velocity. Symp. Int. Combust. **4**(1), 450–457 (1953)
11. Bykov, V., Goldfarb, I., Gol'dshtein, V., Kagan, L., Sivashinsky, G.: Effects of hydraulic resistance and heat losses on detonability and flammability limits. Combust. Theory Model. **8**(2), 413–424 (2004)
12. Chao, J., Lee, J.H.S.: The propagation mechanism of high speed turbulent deflagrations. Shock Waves **12**, 277–289 (2003)
13. Chase, M.W., Curnutt, J.L., Downey, J.R., Jr., McDonald, R.A., Syverud, A.N., Valenzuela, E.A.: Janaf thermochemical tables, 1982 supplement. J. Phys. Chem. Ref. Data **11**(3), 695–940 (1982)
14. Ciccarelli, G., Dorofeev, S.: Flame acceleration and transition to detonation in ducts. Prog. Energy Combust. Sci. **34**(4), 499–550 (2008)

15. Courant, R., Friedrichs, K.O.: Supersonic Flows and Shock Waves. Interscience, New York (1948)
16. Cowie, L.L., Rybicki, G.B.: The structure and evolution of galacto-detonation waves: some analytic results in sequential star formation models of spiral galaxies. ApJ **260**(2), 504–511 (1982)
17. Curran, E.T., Heiser, W.H., Pratt, D.T.: Fluid phenomena in scramjet combustion systems. Annu. Rev. Fluid Mech. **28**(1), 323–360 (1996)
18. Dabora E.K., Nicholls J.A., Morrison R.B.: The influence of a compressible boundary on the propagation of gaseous detonations. Symp Int Combust **10**(1), 817–830 (1965)
19. Davis, W.C., Fickett, W.: Detonation. University of California Press, Berkeley (1979)
20. Dionne, J.-P.: Numerical study of the propagation of non-ideal detonations, PhD Thesis, McGill University, Montreal (2000)
21. Dionne, J.P., Duquette, R., Yoshinaka, A., Lee, J.H.S.: Pathological Detonations in H_2-Cl_2. Combust. Sci. Technol. **158**(1), 5–14 (2000)
22. Dionne, J.-P., Ng, H.D., Lee, J.H.S.: Transient development of friction-induced low-velocity detonations. Proc. Combust. Inst. **28**(1), 645–651 (2000)
23. Döring, W.: Über den detonationsvorgang in gasen. Ann. Phys. **435**(6–7), 421–436 (1943)
24. Duff, R.E.: Calculation of reaction profiles behind steady-state shock waves. I. Application to detonation waves. J. Chem. Phys. **28**(6), 1193–1197 (1958)
25. Edwards, D.H., Brown, D.R., Hooper, G., Jones, A.T.: The influence of wall heat transfer on the expansion following a C-J detonation wave. J. Phys. D: Appl. Phys. **3**(3), 365–376 (1970)
26. Erpenbeck, J.J.: Steady quasi-one-dimensional detonations in idealized systems. Phys. Fluids **12**(5), 967–982 (1969)
27. Eyring, H., Powell, R.E., Duffy, G.H., Parlin, R.B.: The stability of detonation. Chem. Rev. **45**(1), 69–181 (1949)
28. Fay, J.A.: Two-dimensional gaseous detonations: Velocity deficit. Phys. Fluids **2**(3), 283–289 (1959)
29. Freedman, W.L., Madore, B.F., Mehta, S.: Galactic detonation waves numerical models illustrating the transition from deterministic to stochastic. ApJ **282**(2), 412–426 (1984)
30. Frost, D., Zhang, F.: Slurry detonation. In: Zhang, F. (ed.) Heterogeneous Detonation, Shock Wave Science and Technology Reference Library, vol. 4, pp. 169–216. Springer, Berlin (2009)
31. Fujiwara, T., Tsuge, S: Quasi-onedimensional analysis of gaseous free detonations. J. Phys. Soc. Jpn. **33**(1), 237–241 (1972)
32. Gelfand, B.E., Frolov, S.M., Nettleton, M.A.: Gaseous detonations – a selective review. Prog. Energy Combust. Sci. **17**(4), 327–371 (1991)
33. Gerola, H., Seiden, P.E.: Stochastic star formation and spiral structure of galaxies. ApJ **223**, 129–135 (1978)
34. Gordon, S., McBride, B.J.: Computer program for computation of complex chemical equilibrium compositions, rocket performance, incident and reflected shocks, and Chapman-Jouguet detonations. Technical Report NASA SP-273, NASA (1971)
35. Gordon, P.V., Sivashinsky, G.I.: Pressure diffusivity and low-velocity detonation. Combust. Flame **136**(4), 440–444 (2004)

36. Gross, R., Oppenheim, A.K.: Recent advances in gaseous detonation. ARS J. **29**, 173–179 (1959)
37. Guenoche, H., Le Diuzet, P., Sedes, C.: Influence of the heat-release function on the detonation states. In: Bowen, J.R., Manson, N.N., Oppenheim, A.K. (eds.) Gasdynamics of Detonations and Explosions. Progress in Astronautics and Aeronautics, vol. 75, pp. 387–407. AIAA, VA (1981)
38. He, L., Clavin, P.: On the direct initiation of gaseous detonations by an energy source. J. Fluid Mech. **277**, 227–248 (1994)
39. Hertzberg, A., Bruckner, A.P., Knowlen, C.: Experimental investigation of ram accelerator propulsion modes. Shock Waves **1**, 17–25 (1991)
40. Heuze, O.: 1899–1909: The Key Years of the Understanding of Shock Wave and Detonation Physics. AIP Conf. Proc. **1195**(1), 311–314 (2009)
41. Jones, H.: A theory of the dependence of the rate of detonation of solid explosives on the diameter of the charge. Proc. R. Soc. Lond. Ser A. Math. Phys. Sci. **189**(1018), 415–426 (1947)
42. Jouguet, E.: Mécanique des explosifs, étude de dynamique chimique. O. Doin & Fils, Paris (1917)
43. Kagan, L., Sivashinsky, G.: The transition from deflagration to detonation in thin channels. Combust. Flame **134**(4), 389–397 (2003)
44. Kirkwood, J.G., Wood, W.W.: Structure of a steady-state plane detonation wave with finite reaction rate. J. Chem. Phys. **22**(11), 1915–1919 (1954)
45. Klein, R., Krok, J.C., Shepherd, J.E.: Curved quasi-steady detonations: Asymptotic analysis and detailed chemical kinetics. Technical Report FM95-04, Graduate Aeronautical Laboratories, California Institute of Technology (1995)
46. Knystautas, R., Lee, J.H.: Detonation parameters for the hydrogen-chlorine system. In: Kuhl, A.L., Bowen, J.R., Leyer, J.C., Borisov, A.A. (eds.) Dynamics of Explosions. Progress in Astronautics and Aeronautics, vol. 114, pp. 32–44. AIAA, VA (1988)
47. Kolesnikov, S., Utkin, A.: Nonclassical steady-state detonation regimes in pressed TNETB. Combust. Explos. Shock Waves **43**, 710–716 (2007)
48. Krehl, P.O.K.: History of Shock Waves, Explosions and Impact: A Chronological and Biographical Reference. Springer, Berlin (2009)
49. Laffitte, P.: Recherches expérimentales sur l'onde explosive et l'onde de choc. Ann. Phys. **10**(4) 623–634 (1925)
50. Lee, J.H., Lee, B.H.K., Shanfield, I.: Two-dimensional unconfined gaseous detonation waves. 10th Symp. (Int.) Combust. **10**(1), 805–815 (1965)
51. Lee J.H.S.: The Detonation Phenomenon. Cambridge University Press, Cambridge (2008)
52. Lee, J.H.S., Moen, I.O.: The mechanism of transition from deflagration to detonation in vapor cloud explosions. Prog. Energy Combust. Sci. **6**(4), 359–389 (1980)
53. Makris, A.: The Propagation of Gaseous Detonations in Porous Media. PhD Thesis, McGill University, Montreal (2003)
54. Makris, A., Shafique, H., Lee, J., Knystautas, R.: Influence of mixture sensitivity and pore size on detonation velocities in porous media. Shock Waves **5**(1), 89–95 (1995)

55. Manson, N., Dabora, E.: Chronology of research on detonation waves: 1920–1950. In: Kuhl, A.L., Leyer, J.C., Borisov, A.A., Sirignano, W.A. (eds.) Dynamic Aspects of Detonations. Progress in Astronautics and Aeronautics, vol. 153, pp. 3–39. AIAA, VA (1993)
56. McBride, B.J., Gordon, S.: Computer program for calculation of complex chemical equilibrium compositions and applications II. Users manual and program description. Technical Report NASA RP-1311, NASA (1996)
57. Mikhel'son, V.A.: On the normal ignition velocity of explosive gaseous mixtures. Scientific Papers of the Moscow Imperial University on Mathematics and Physics **10**, 1–93 (1893)
58. von Neumann, J.: Theory of detonation waves. Technical Report OSRD-549, National Defense Research Committee (1942)
59. von Neumann, J.: Theory of Detonation Waves, John von Neumann: Collected Works, 1903–1957, vol. 6, pp. 178–218. Pergamon Press, Oxford (1963)
60. Nikolaev, Yu.A., Fomin, P.A.: Analysis of equilibrium flows of chemically reacting gases. Combust. Explos. Shock Waves **18**(1), 53–58 (1982)
61. Oran, E.S.: Astrophysical combustion. Proc. Combust. Inst. **30**(2), 1823–1840 (2005)
62. Oran, E.S., Boris, J.P.: Numerical Simulation of Reactive Flow. Cambridge University Press, Cambridge (2001)
63. Paillard, C., Dupre, G., Lisbet, R., Combourieu, J., Fokeev, V.P., Gvozdeva, L.G.: A study of hydrogen azide detonation with heat transfer at the wall. Acta Astronaut. **6**(3–4), 227–242 (1979)
64. Parker, E.N.: Dynamics of the interplanetary gas and magnetic fields. ApJ **128**, 664–676 (1958)
65. Peraldi, O., Knystautas, R., Lee, J.H.: Criteria for transition to detonation in tubes. 21st Symp. (Int.) Combust. **21**(1), 1629–1637 (1988)
66. Pinaev, A.V., Lyamin, G.A.: Fundamental laws governing subsonic and detonating gas combustion in inert porous media. Combust. Explos. Shock Waves **25**(4), 448–458 (1989)
67. Powers, J., Paolucci, S.: Accurate spatial resolution estimates for reactive supersonic flow with detailed chemistry. AIAA J. **43**, 1088–1099 (2005)
68. Radulescu, M.I.: The propagation and failure mechanism of gaseous detonations: Experiments in porous-walled tubes. PhD Thesis, McGill University, Montreal (2003)
69. Radulescu, M.I., Hanson, R.K.: Effect of heat loss on pulse-detonation-engine flow fields and performance. J. Propul. Power **21**(2), 274–285 (2005)
70. Radulescu, M.I., Lee, J.H.S.: The failure mechanism of gaseous detonations: Experiments in porous wall tubes. Combust. Flame **131**(1–2), 29–46 (2002)
71. Radulescu, M.I., Sharpe, G.J., Law, C.K., Lee, J.H.S.: The hydrodynamic structure of unstable cellular detonations. J. Fluid Mech. **580**, 31–81 (2007)
72. Rozing, V.O., Khariton, Yu.B.: The detonation cutoff of explosive substances when the charge diameters are small. Dokl. Akad. Nauk. SSSR **26**(4), 360–361 (1940)
73. Sasoh, A., Knowlen, C.: Ram accelerator operation analysis in thermally choked and transdetonative propulsive modes. Trans. Jpn. Soc. Aeronaut. Space Sci. **40**(128), 130–148 (1997)
74. Shapiro, A.H.: The Dynamics and Thermodynamics of Compressible Fluid Flow, vol. 1. Ronald Press, New York (1953)

75. Sharpe, G.J.: Linear stability of pathological detonations. J. Fluid Mech. **401**, 311–338 (1999)
76. Sharpe, G.J.: The structure of planar and curved detonation waves with reversible reactions. Phys. Fluids **12**(11), 3007–3020 (2000)
77. Sharpe, G.J., Falle, S.A.E.G.: One-dimensional nonlinear stability of pathological detonations. J. Fluid Mech. **414**, 339–366 (1999)
78. Shchelkin, K.I.: Influence of the tube walls roughness on the onset and propagation of detonation in gases. Zh. Eksp. Teor. Fiz. **10**, 823–827 (1940)
79. Sichel, M., David, T.S.: Transfer behind detonations in H_2-O_2 mixtures. AIAA J. **4**(6), 1089–1090 (1966)
80. Skinner, J.H., Jr.: Friction and heat-transfer effects on the nonsteady flow behind a detonation. AIAA J. **5**(11), 2069–2071 (1967)
81. Sleath, J.P., Alexander, P.: A new model of the structure of spiral galaxies based on propagating star formation – I. The galactic star formation rate and Schmidt Law. Mon. Not. R. Astron. Soc. **275**, 507–514 (1995)
82. Sokolik, A.S., Shchelkin, K.I.: Detonation in gas mixtures: The influence of pressure on the velocity of a detonation wave. Acta Physicokhimika SSSR **1**, 311–317 (1934)
83. Sommers, W.P.: Gaseous detonation wave interactions with nonrigid boundaries. ARS J. **31**, 1780–1782 (1961)
84. Sommers, W.P., Morrison, R.B.: Simulation of condensed-explosive detonation phenomena with gases. Phys. Fluids **5**(2), 241–248 (1962)
85. Spalding, D.B.: A theory of inflammability limits and flame-quenching. Proc. R. Soc. Lond. Ser A. Math. Phys. Sci. **240**(1220), 83–100 (1957)
86. De Sterck, H.: Critical point analysis of transonic flow profiles with heat conduction. SIAM J. Appl. Dyn. Syst. **6**, 645–662 (2007)
87. Strehlow, R.A.: Fundamentals of Combustion. International Textbook Co., Scranton, PA (1968)
88. Tanguay, V., Higgins, A.J.: On the inclusion of frictional work in nonideal detonations. In: Shepherd, J.E. (ed.) 20th International Colloquium on the Dynamics of Explosions and Reactive Systems: Extended Abstracts and Technical Program (2005). ISBN 1600490018, 9781600490019 (CD-ROM)
89. Tanguay, V., Higgins, A.J., Zhang, F.: A simple analytical model for reactive particle ignition in explosives. Propellants Explos. Pyrotech. **32**(5), 371–384 (2007)
90. Tarver, C.M.: Multiple roles of highly vibrationally excited molecules in the reaction zones of detonation waves. J. Phys. Chem. A **101**(27), 4845–4851 (1997)
91. Tarver C.M.: On the existence of pathological detonation waves. AIP Conf. Proc. **706**, 902 (2004). doi: 10.1063/1.1780383
92. Tarver, C., Forbes, J., Urtiew, P.: Nonequilibrium Zeldovich-von Neumann-Doring theory and reactive flow modeling of detonation. Russ. J. Phys. Chem. B Focus Phys. **1**(1), 39–45 (2007)
93. Taylor, G.I.: The dynamics of the combustion products behind plane and spherical detonation fronts in explosives. Proc. R. Soc. Lond. Ser A. Math. Phys. Sci. **200**(1061), 235–247 (1950)
94. Trubachev, A.: Detonation waves in interstellar gas. Combust. Explos. Shock Waves **33**, 72–76 (1997)

95. Tsuge, S., Furukawa, H., Matsukawa, M., Nakagawa, T.: On the dual properties and the limit of hydrogen-oxygen free detonations waves. Astronaut. Acta **15**, 377–386 (1970)
96. Utkin, A.V., Kolesnikov, S.A., Pershin, S.V.: Effect of the initial density on the structure of detonation waves in heterogeneous explosives. Combust. Explos. Shock Waves **38**(5), 590–597 (2002)
97. Vasil'ev, A.A., Zak, D.V.: Detonation of gas jets. Combust. Explos. Shock Waves **22**(4), 463–468 (1986)
98. Vieille, P.: Rôle des discontinuités dans la propagation des phénomènes explosifs. C. R. Acad. Sci., **130**, 413–416 (1900)
99. Vincenti, W.G., Kruger, C.H.: Introduction to Physical Gas Dynamics. Krieger, Malabar, FL (1965)
100. Wecken, F.: Non-ideal detonation with constant lateral expansion. In: Fourth Symposium (International) on Detonation, pp. 107–116 (1965)
101. Wood, W.W., Kirkwood, J.G.: Diameter effect in condensed explosives. The relation between velocity and radius of curvature of the detonation wave. J. Chem. Phys. **22**(11), 1920–1924 (1954)
102. Wood, W.W., Kirkwood, J.G.: On the existence of steady-state detonations supported by a single chemical reaction. J. Chem. Phys. **25**(6), 1276–1277 (1956)
103. Wood, W.W., Parker, F.R.: Structure of a centered rarefaction wave in a relaxing gas. Phys. Fluids **1**(3), 230–241 (1958)
104. Wood, W.W., Salsburg, Z.W.: Analysis of steady-state supported one-dimensional detonations and shocks. Phys. Fluids **3**(4), 549–566 (1960)
105. Yao, J., Stewart, D.S.: On the normal detonation shock velocity-curvature relationship for materials with large activation energy. Combust. Flame **100**(4), 519–528 (1995)
106. Zel'dovich, Ya.B.: On the theory of the propagation of detonations on gaseous system. Zh. Eksp. Teor. Fiz. **10**(5), 542–568 (1940)
107. Zel'dovich, Ya.B., Kompaneets, A.S.: Theory of Detonation. Academic, New York (1960)
108. Zel'dovich, Ya.B., Ratner, S.B.: Zh. Eksp. Teor. Fiz. **11**, 170 (1941)
109. Zel'dovich, Ya.B., Gel'fand, B.E., Kazhdan, Ya.M., Frolov, S.M.: Detonation propagation in a rough tube taking account of deceleration and heat transfer. Combust. Explos. Shock Waves **23**, 342–349 (1987)
110. Zel'dovich, B., Borisov, A.A., Gelfand, B.E., Frolov Ya, S.M., Mailkov, A.E.: Nonideal detonation waves in rough tubes. In: Kuhl, A.L., Bowen, J.R., Leyer, J.C., Borisov, A.A. (eds.) Dynamics of Explosions. Progress in Astronautics and Aeronautics, vol. 114, pp. 211–231. AIAA, VA (1988)
111. Zhang, F.: Detonation in reactive solid particle-gas flow. J. Propuls. Power **22**, 1289–1309 (2006)
112. Zhang, F.: Detonation of gas-particle flow. In: Zhang, F. (ed.) Heterogeneous Detonation, Shock Wave Science and Technology Reference Library, vol. 4, pp. 87–168. Springer, Berlin (2009)

http://www.springer.com/978-3-642-22966-4

Shock Waves Science and Technology Library, Vol. 6
Detonation Dynamics
Zhang, F. (Ed.)
2012, XVIII, 470 p., Hardcover
ISBN: 978-3-642-22966-4